



FEDERAL UNIVERSITY OF ABC - UFABC
NANOSCIENCE AND ADVANCED MATERIALS
GRADUATE PROGRAM

João Henrique Quintino Palhares

Effect of doping in tantalum oxide-based resistive switching
devices (Memristors)

Santo André, SP, Brazil
2020

João Henrique Quintino Palhares

Effect of doping in tantalum oxide-based resistive switching
devices (Memristors)

Dissertation presented to the Nanosciences and
Advanced Materials Graduate Program of the
Federal University of ABC as partial requirement to
obtain the title of Master of Nanosciences and
Advanced Materials.

Supervisor: André Santarosa Ferlauto

Santo André, SP, Brazil
2020

Sistema de Bibliotecas da Universidade Federal do ABC
Elaborada pelo Sistema de Geração de Ficha Catalográfica da UFABC
com os dados fornecidos pelo(a) autor(a).

Palhares, João Henrique Quintino

Effect of doping in tantalum oxide-based resistive switching devices
(Memristors) / João Henrique Quintino Palhares. — 2020.

71 fls. : il.

Orientador: André Santarosa Ferlauto

Dissertação (Mestrado) — Universidade Federal do ABC, Programa de Pós-Graduação em Nanociências e Materiais Avançados, Santo André, 2020.

1. Resistive memories. 2. Memristors. 3. Pulsed Laser Deposition (PLD). 4. Tantalum oxide. 5. Zirconium doping. I. Ferlauto, André Santarosa. II. Programa de Pós-Graduação em Nanociências e Materiais Avançados, 2020. III. Título.

Este exemplar foi revisado e alterado em relação à versão original, de acordo com as observações levantadas pela banca no dia da defesa, sob responsabilidade única do(a) autor(a) e com a anuência do(a) orientador(a).

de

de

Assinatura do(a) autor(a):

 _____

Assinatura do(a) orientador(a):

 _____



SIGAA - Sistema Integrado de Gestão de Atividades Acadêmicas
UFABC - Fundação Universidade Federal do ABC
Programa de Pós-Graduação em Nanociências e Materiais Avançados
CNPJ nº 07.722.779/0001-06
Av. dos Estados, 5001 - Bairro Santa Terezinha - Santo André - SP - Brasil
ppg.nanomat@ufabc.edu.br



FOLHA DE ASSINATURAS

Assinaturas dos membros da Banca Examinadora que avaliou e aprovou a Defesa de Dissertação de Mestrado do candidato JOÃO HENRIQUE QUINTINO PALHARES, realizada em 14 de Agosto de 2020:

Dr. ANDRE SANTAROSA FERLAUTO, UFABC

Presidente - Interno ao Programa

Dr. EVERTON BONTURIM UPM

Membro Titular - Examinador(a) Externo ao Programa

Dr. ALEXANDRE JOSE DE CASTRO LANFREDI, UFABC

Membro Titular - Examinador(a) Interno ao Programa

Dr. GUSTAVO MARTINI DALPIAN, UFABC

Membro Suplente - Examinador(a) Interno ao Programa

Dr. RODRIGO GRIBEL LACERDA

Membro Suplente - Examinador(a) Externo à Instituição

Abstract

Resistive switching (RS) devices (memristors) based on ionic carriers have attracted attention due to their simple structure (only two terminals), low energy consumption, high scalability, endurance, and possibility of novel computing architectures. However, variability is still a limiting factor for RS applications. In oxide-based RS devices, the reversible change (switching) in the resistance of a thin dielectric layer results from movement of oxygen vacancies induced by high electric fields. To reduce variability, better understanding and control of oxygen vacancy formation and movement is paramount. In this work, the intrinsic and extrinsic doping of tantalum oxide layers in RS devices was investigated. Pure and Zr-doped tantalum oxide thin films were prepared by pulsed laser deposition (PLD) and characterized by atomic force microscopy (AFM), x-ray photoelectron spectroscopy (XPS), and spectroscopic ellipsometry (SE) to evaluate surface morphology, film thickness, stoichiometry, electronic structure, and presence of defects. The pure and Zr-doped films were amorphous and had smooth surface. SE reveals that Zr addition promotes a sub-gap optical absorption that can be associated with increased concentration of oxygen vacancies. In pure tantalum oxide films, a similar effect can be achieved by reducing the oxygen partial pressure during deposition. RS devices were micropatterned by photolithography using dog-bone and common bottom contact architectures. The device response was analyzed using an electronic hopping transport model that enables determination of defect (trap) concentration, which should be proportional to the O vacancy concentration. Such analysis confirms the SE results that Zr doping promotes O vacancy formation. Systematic electrical parametrization shows that Zr-doped devices are more reliable, have a higher resistance window, higher yield, and lower forming voltage, which might be ascribed to doping effects on filament confinement and oxygen vacancy formation. This study suggests that Zr doping of tantalum oxide memristor is a promising vacancy engineering strategy to tune memristor performance.

Keywords: resistive switching devices, tantalum oxide, thin films, pulsed laser deposition, doping, neuromorphic devices, oxygen vacancy.

Resumo

Os dispositivos de comutação resistiva (RS) (memristores) baseados em portadores iônicos chamaram a atenção devido à sua estrutura simples (apenas dois terminais), baixo consumo de energia, alta escalabilidade, endurance e possibilidade de novas arquiteturas de computação. Contudo, a variabilidade é ainda um fator limitante para as aplicações RS. Nos dispositivos RS à base de óxido, a mudança reversível (comutação) na resistência de uma fina camada dielétrica resulta do movimento de vacâncias de oxigênio induzidas por campos elétricos elevados. Para reduzir a variabilidade, é primordial entender e controlar a formação e movimentação de vacâncias de oxigênio. Neste trabalho, foi investigada a dopagem intrínseca e extrínseca das camadas de óxido de tântalo em dispositivos RS. Películas finas de óxido de tântalo puro e Zr-doped foram preparadas por deposição laser pulsada (PLD) e caracterizadas por microscopia de força atômica (AFM), Espectroscopia de fotoelétrons excitados por raios X (XPS), e elipsometria espectroscópica (SE) para avaliar a morfologia da superfície, espessura dos filmes, estequiometria, estrutura eletrônica, e presença de defeitos. As películas puras e dopadas com Zr eram amorfas e tinham uma superfície lisa. A análise por elipsometria revela que a adição de Zr promove uma absorção ótica no sub-gap que pode ser associada com o aumento da concentração de vacâncias de oxigênio. Nas películas de óxido de tântalo puro, um efeito semelhante pode ser alcançado reduzindo a pressão parcial de oxigênio durante a deposição. Os dispositivos RS foram microfabricados por fotolitografia utilizando arquiteturas do tipo dog-bone e eletrodo de fundo comum. A resposta do dispositivo foi analisada utilizando um modelo hopping de transporte eletrônico que permite determinar a concentração de defeitos (armadilhas), que deve ser proporcional à concentração de vacâncias de oxigênio. Tal análise confirma os resultados do SE que a dopagem Zr promove a formação de vacâncias. A parametrização elétrica sistemática mostra que os dispositivos dopados com Zr são mais fiáveis, têm uma maior janela de resistência, maior rendimento, e menor tensão de formação, que pode ser atribuída a efeitos de dopagem no confinamento do filamento e formação de vacância de oxigênio. Este estudo sugere que a dopagem com Zr do memristor de óxido de tântalo é uma estratégia de engenharia de vacância promissora para melhorar o desempenho do memristor.

Palavras-chave: dispositivos de chaveamento resistivo, óxido de tântalo, memristor, filmes finos, deposição por laser pulsado, dopagem, dispositivos neuromórficos, vacância de oxigênio

Acknowledgement

This study was financed in part by the Coordenação de Aperfeiçoamento de Pessoal de Nível Superior - Brasil (CAPES) - Finance Code 001.

O presente trabalho foi realizado com apoio da Coordenação de Aperfeiçoamento de Pessoal de Nível Superior - Brasil (CAPES) - Código de Financiamento 001.

É com alegria que venho agradecer todas as pessoas que de forma direta ou indireta me ajudaram a alcançar mais essa vitória na minha vida, mais uma etapa em busca do conhecimento e do sonho de entender as coisas e contribuir com a ciência. Compartilho essa vitória com minha mãe Célida, maravilhosa, e ao meu pai querido, Paulo, exemplos pra mim. Essa conquista é nossa. Obrigado por dar toda a força ao que eu escolhi fazer da vida, e por tentar entender, me agradar e ajudar com o que podem e o que não podem pra eu ser feliz na vida. Sem vocês a realização desse sonho não seria possível, vocês são os principais responsáveis por essa conquista. Amo muito vocês!

Obrigado ao meu avô querido, que hoje está com 104 anos, e a minha querida avó. Obrigado por colocar minha mãezinha no mundo e eu também, por assim dizer.

A minha esposa linda e inteligente, Rafaela. A minha sogra Eni, meu sogro Donizete e minha cunhada Renata e Daniel. Obrigado esposa, por sempre me apoiar e estar do meu lado nesse projeto e por aceitar dividir o meu amor e tempo com a ciência. Obrigado pela paciência, força, carinho e amor. Amo muito você! Obrigado por crescer comigo e por aceitar se casar comigo.

Agradeço aos meus irmãos queridos e amigos Filipe e Matheus e minhas cunhadinhas queridas Cris e Fê, e finalmente aos meus sobrinhos bagunceiros: Davi, Larinha e Sarinha. Obrigado por trazerem encanto a vida da nossa família, por serem exemplos de carinho, afeto e amor sincero. Amo vocês família.

Agradeço aos meus amigos e colegas que fiz durante todas as minhas experiências de pesquisa: Ao meu amigo Wellington que dividiu laboratório comigo por tantos anos, obrigado por todos os ensinamentos. A todas as pessoas que me ajudaram no departamento de física da UFMG, por todo tempo que passei trabalhando por lá: Fabiano, Padua, prof. Juan, Rafael, prof. Bernardo, Thales. Ao pessoal do laboratório ao qual faço parte, o LAMEN, da UFABC: Fabi, Renata, Victor, Lucas, Natali, Rafael e aos novos integrantes. Grande abraço a todos! Ao meus amigos da simulação da UFABC por todos momentos e companhias: Pedro japa, Jhonatan, Matheus, Pedro paulista.

Aos meus mentores: Prof. André Ferlauto, que considero como um amigo, e pai na pesquisa. Me ensinou tudo que sei sobre filmes finos. Obrigado pela força, paciência e por aceitar me orientar nesse projeto. Espero continuar colaborando e aprendendo com o senhor. Aos professores que conheci nesse meio tempo em São Paulo, prof. Daniel, prof. Fabio e toda equipe do IPEN, em especial ao prof. Everton pela gentileza e paciência em me treinar no PLD. Agradeço aos outros mentores que tive oportunidade de trabalhar e que transformaram a minha vida: ao professor Gilberto, por todos os ensinamentos, por apostar em mim e por abrir várias portas: oportunidades de iniciação científica, de estágio e de pesquisa no Centro de Microscopia. Obrigado também ao professor Wagner, ao Doug e ao pessoal do CM. I also would like to thank my dear professor Nancy, for always willing to help me. Thanks for the opportunity you gave me to work in your Lab at University of Florida, it was a transformative experience that changed my life completely. Thanks prof. Charit also for all the opportunities and support during my stay at University of Idaho.

Finally, thanks to my colleagues and supervisors here at Université de Sherbrooke: Prof. Yann, prof. Dominique and prof. Fabien. Thanks for being patient, thanks for all the teachings and for the opportunity that was given to me to here at 3IT-UDES. It is being such a transformative experience that I hope to continue having here. Merci!

Gostaria de agradecer aos meus amigos que considero como irmãos: Carlos (Carlitos), e Guilherme (Gui) por serem meus grandes amigos. Obrigado por todos momentos de felicidade que marcaram minha vida. Obrigado também as suas companheiras que são minhas amigas e irmãs também: Gabi e Verônica. Saudades de vocês, grande abraço!

Obrigado La Cabane! Obrigado aos amigos que fiz na quarentena, obrigado por toda força e carinho. Vocês foram a força minha e da Rafa nessa quarentena: René, Geandra, Jéssica, Jansller, Aliny, Pier Luc, Malo.

Por último, obrigado CAPES e UFABC por apoiar e apostar no sonho de tantos jovens como eu que querem aprender e transformar o mundo a partir do conhecimento. Obrigado as pessoas por trás dessas políticas de incentivo a educação e a pesquisa, que vocês continuem fortes apesar dos tempos difíceis. Espero um dia poder contribuir com o fortalecimento dessas instituições.

"If there are no fruits, it was worth the beauty of the flowers; if there are no flowers, it was worth the shadow of the leaves; if there are no leaves, it was worth the intention of the seed."

"Se não houver frutos, valeu a beleza das flores; se não houver flores, valeu a sombra das folhas; se não houver folhas, valeu a intenção da semente."

Mauricio Francisco Ceolin

Content

1.Introduction	15
2.Literature review	17
2.1. Resistive Switching	17
2.2. Types of RS	18
2.3 Oxide based RS Devices: Valence change mechanism	19
2.4. RS Devices Basic Operations types	20
2.5. BRS Operation Parameters	21
2.6. Tantalum oxide-based RS Devices	22
2.7. Doping Effects on oxide-based ReRAM devices	23
2.8. Bi-layered oxide-based ReRAM devices	24
2.9. Electronic transport in tantalum oxide-based ReRAM devices.....	25
3. Objectives	26
3.1. General Objectives	26
3.2. Specific objectives	26
4. Materials and methods.....	27
4.1. Target manufacturing	27
4.2 Thin-Film preparation and characterization	28
4.2.1. Pulsed Laser Deposition	28
4.2.2. Chemical characterization	29
4.2.3. Thin film Optical properties	29
4.2.4. Thin film surface topography.....	29
4.3. Thin-film Preparation of the Resistive Switching Devices	29
4.4. RS Device micro-fabrication process.....	31
4.5 Device Electrical parametrization.....	34
4.6 Electronic transport analysis.....	35
5. Results and discussions	37
5.1 Thin film surface.....	39
5.2 Chemical analysis	40
5.3 Thin film Optical properties	42
5.4. Device electrical parametrization.....	44
5.4.1 Switching characteristics of type I devices.....	45

5.4.2 Switching characteristics of type II devices	48
5.4.3 Electronic transport analysis.....	51
5.4 Doping effect on vacancy concentration and switching operation parameters	53
5.6 Multi-state analog switching.....	56
6.Conclusion	59
A.Appendices	61
Bibliography	63

List of figures

Figure 1: The fourth fundamental two terminal electronic components and its fundamental pair of variables. In the case of the memristor it is flux and charge. Figure taken from Ref.[13].	17
Figure 2: The well-known resistive switching types are a) phase change mechanism, b) electrochemical mechanism, c) valence change mechanism.	19
Figure 3: I-V characteristic curve (sweep test) of a typical a) Bipolar resistive switching device, b) Unipolar Resistive switching device and c) Complementary Resistive Switching device.	21
Figure 4: Typical I-V sweep curve of a RS device.	22
Figure 5: The bipolar characteristic after sweep cycles on a) Single layer and b) bi-layered RRAM devices.[17]	24
Figure 6: a) Pulsed Laser Deposition System, b) tantalum oxide based and mixed zirconia and tantalum oxide targets.	28
Figure 7: Structure stacks I and II. For structure type I the main layer is deposited at low oxygen pressure pO_2 ($pO_2 = 10^{-3}$ mbar) and is used as an oxygen vacancy source. A thinner (12-14 nm) layer, deposited at oxygen rich atmosphere that yields a close to stoichiometric Ta_2O_5 composition. In the devices with structure type II, an active 10 nm-thick layer is prepared with an intermediate oxygen pressure ($pO_2=10^{-2}$ mbar) and capped with very thin passivation layer (<1 nm) deposited at $pO_2=1 \times 10^{-1}$ mbar.	31
Figure 8: Device stack schematic of dot pad type devices (a-c) and dog-bone (d-f) devices: (a) silicon substrate; (b) tungsten bottom electrode (BE); layered oxygen poor and oxygen rich tantalum oxide (for the pure and the ZrO_2 doped target) memristive cell; (c) micropatterned tungsten top electrode (TE). d) micropatterned tungsten bottom electrode, e) memristive oxide bilayer and f) micropatterned top electrode.	32
Figure 9: Dog-bone device fabrication schematics: (a) After developing photoresist mask bottom electrode, followed by (b) deposition of tungsten and afterwards lift-off process. Right after, (c)(d) another mask was also prepared for PLD deposited oxide active layer. After that, (e)(f) photoresist mask for top electrode were also prepared over both bottom and active layer to deposit tungsten top electrode.	33
Figure 10: Clean room facility for micropatterning of the photoresist mask: a) Microtech Laserwriter model LW405 b) Spinner Laurell model WS-650SZ.	34

Figure 11:Device parametrization and testing using a a) 4 probe westwood probestation b) keysight B1500 and a c) Device under test (DUT) testing setup scheme with two source meter units (SMUs) for voltage and current measurement (Sense High, Sense Low) and voltage application (Force High, Force Low)	35
Figure 12:AFM analysis of the Zr doped Tantalum oxide thin films prepared with oxygen partial pressure of a) 5×10^{-3} , b) 2×10^{-2} and c) 1×10^{-1} mbar.....	39
Figure 13:AFM analysis of the Tantalum oxide thin film prepared with oxygen partial pressure of 1×10^{-1} mbar.....	40
Figure 14:SEM image of the pure tantalum oxide thin film prepared at 1×10^{-1} mbar ...	40
Figure 15:XPS analysis of the sample prepared using a pure tantalum oxide target and pressure of 5×10^{-3} mbar after 30 seconds of plasma etching.	42
Figure 16:Absorption spectra of pure tantalum oxide and Zr doped tantalum oxide thin films prepared at oxygen rich and poor atmosphere pressure.	43
Figure 17:Forming operation for pure tantalum oxide devices (in blue) and Zr doped devices (in red) with 80 μm pad sizes.....	46
Figure 18:I-V switching cycles of a) different cells (#9x5 and #10x3) at the same wafer of 80 μm pad size Zr doped tantalum oxide device structure type Ia and b) 80 μm pad size, cells #13x2 and #13x1 of pure tantalum oxide-based device structure type Ib.....	47
Figure 19:Forming operation for some pure tantalum oxide devices (in blue) and Zr doped devices (in red) with 80 μm pad sizes.....	48
Figure 20:I-V switching cycles of a) 2 different cells (#5x6 and #9x6) of the same die of 80 μm pad size Zr doped tantalum oxide device structure type IIa and b) 80 μm pad size (#4x6 and #5x4) pure tantalum oxide-based device structure type IIb.....	49
Figure 21:Dog-bone type 3 μm x 3 μm Zr doped devices (stack structure type IIa) were tested in order to evaluate effect of reduction on device active area. b) It shows a reliable switching behavior, with LRS value of around 3 k Ω and HRS of 83 k Ω	50
Figure 22: J-E plot of pristine devices along with hopping fit for structure a) Ib and b) Ia with 80 μm and 100 μm pad devices) - a) The devices with pure tantalum oxide films with the limiting layer prepared at 10^{-1} mbar (Ib) have a trap distance going of 3.5 nm for the two pad sizes. On the other hand, remarkably b) for the same structure (Ia) and pressure conditions, devices with Zr-doped layers obtained a lower trap distance value of minimum 1.03 nm and maximum 2.07 nm.	52
Figure 23:The devices with pure tantalum oxide films with the limiting layer prepared at 2×10^{-2} mbar (IIb) have a trap distance going from 1.45 nm to 1.63 nm. On the other hand,	

b) for the same structure (IIa) and pressure conditions, devices with Zr-doped layers obtained a lower trap distance value of minimum 0.83 nm.	53
Figure 24:The devices with pure tantalum oxide films have a trap density of $2.27 \times 10^{19} \text{ cm}^{-3}$ (type I) and $2.73 \times 10^{20} \text{ cm}^{-3}$ (type II). Such variation is associated with the difference in the oxygen stoichiometry and partial reduction of the active layer in both devices that were produced using different oxygen partial pressures. These values are similar to those obtained by Gritensko et al (in purple) of $1.9 \times 10^{19} \text{ cm}^{-3}$ and $3 \times 10^{20} \text{ cm}^{-3}$ by using the Phonon assisted trap tunneling (PATT) model to adjust device IxV curves [50]. Interestingly, for the devices with Zr-doped layers the obtained trap density values are larger, $2.45 \times 10^{20} \text{ cm}^{-3}$ and $1.33 \times 10^{21} \text{ cm}^{-3}$ for device type I and II, respectively.	54
Figure 25:Forming voltage values of extrinsic doped films (Zr doping – Ia and IIa) and intrinsic doped ones (IIa) presented lower forming voltage of $-0.8\text{V} \pm 0.16\text{V}$, $-1.89\text{V} \pm 0.75\text{V}$, $-0.803\text{V} \pm 0.098\text{V}$, respectively, compared to the device based on the stoichiometric film structure type Ib of $-7.475\text{V} \pm 1.59\text{V}$	55
Figure 26: Zr doped devices prepared at both oxygen partial pressure conditions 10^{-1} mbar (O_2 rich) and 2×10^{-2} mbar (O_2 poor) presented a higher resistance window of 23.8 ± 3.58 and 9.63 ± 1.61 for oxygen poor and rich condition, compared to pure tantalum oxides structure that have a mean resistance window ranging of 7.74 ± 3.56 and 5.69 ± 2.09 for oxygen poor and rich condition Ta based devices.	56
Figure 27:Analog gradual switching operations observed in a) Zr doped devices in negative RESET operations and b) in pure tantalum oxide devices in positive SET operations.	57
Figure 28:X-ray diffraction pattern of the a) pure tantalum oxide using a copper x-ray target source and b) 20%wt zirconium oxide and 80% tantalum oxide powder mixture after sintering using molybdenum target source.	61
Figure 29:I-V switching cycles of a) 2 different cells (5x1 and 3x1) at the same die of 100 μm pad size Zr doped tantalum oxide device structure type Ia and b) 100 μm (4x1 and 4x2) pure tantalum oxide-based device structure type Ib.	62

List of Tables

Table 1: Device stack description of structures type I and II. pO_2 used to deposit the oxide and thickness are represented in parenthesis.	31
Table 2:The AFM analysis of a projected surface area of $0.25 \mu m^2$ of the pure and mixed tantalum oxide thin films.....	39
Table 3:The oxidation number and respective phase content for the sample etched for 30, 60 and 600 seconds. The XPS survey analysis with the ratio of oxygen and tantalum for the Ta_2O_5 thin film.	42
Table 4:Tantalum oxide and zirconium doped tantalum oxide thin film growth rate for different oxygen partial pressure conditions	44
Table 5:Cycle to cycle variability for devices with stack structure type Ia and Ib with $80 \mu m$ pad sizes. See in the table mean resistance values, relative standard error (RSE), resistance window and forming voltage.....	48
Table 6: Cycle to cycle variability for devices with stack structure type IIa and IIb with $80 \mu m$ pad sizes. See in the table mean resistance values, relative standard error (RSE), resistance window and forming voltage.....	50
Table 7:Tantalum oxide XPS fitting constraints.	61
Table 8:Cycle to cycle variability for devices with stack structure type Ia and Ib with $100 \mu m$ and $80 \mu m$ pad sizes.	62

1. Introduction

Resistive switching (RS) is a physical phenomenon observed in dielectric materials submitted to high electric field or high current levels. The dielectric material (active layer) sandwiched between two metals electrodes suddenly changes its local resistance under voltage or current application[1], [2], [3]. It is passive, and then nonvolatile. It means that it keeps its resistance state after switching without need of permanent voltage application. Resistive switching random access memory (ReRAM) has been considered as a promising technology to replace flash memories. Among all types of resistive switching which are going to be discussed in further sections, the oxide-based ReRAM is the most promising one due to its simplicity and due to the fact that the current storage technology also uses oxides as gate layers and thus processing technology for these materials is more conventional. The resistance change in these devices occurs due to the formation of an oxygen vacancy nanofilament bridging both electrodes under voltage stimuli[4]. The ReRAM device basic structure is a metal–insulator–metal (MIM) stack, which is normally asymmetric, containing one oxidizing electrode (W, Ta, Ti and Hf) and one electrode with a higher work function (Pt, TiN,etc). The non-inert electrode acts as an ohmic interface responsible for the generation of the oxygen vacancy defects. The noble electrode act as a Schottky barrier[5]. Some studies are exploring symmetric structures for neuromorphic applications using the same material for top and bottom electrode[6]. The oxides that are most studied as switching layers are TaO_x, HfO_x, ZnO, TiO [7]. Usually the resistance in the oxide layer can be switched between two resistance values, low resistance state (LRS) and high resistance state (HRS). However, novel stack combinations of materials are showing multiple resistance states that are intermediary between HRS and LRS and thus are being explored as promising candidates for neuromorphic computing[8].

The oxide layer can be deposited by methods such as reactive sputtering, atomic layer deposition, electrochemical deposition, pulsed laser deposition (PLD) etc. In PLD, an UV laser beam vaporizes the target surface onto the substrate. This technique is used to deposit multi-element films with controllable stoichiometry[9]. The concentration of oxygen vacancies, i.e, the stoichiometry, in the oxide can be controlled by adjusting the oxygen partial pressure during thin film growing[10]. It has been named as intrinsic doping. Another way to generate oxygen vacancy defects is adding a foreign atom to the

oxide (extrinsic doping). For tantalum oxide based devices there are only a few examples of extrinsic doping, including Si [11], or Zr [12]. Thus, device performance can be tuned and modulated for different employments by controlling processing parameters, target composition and device stack combinations.

The dissertation is going to cover some of these strategies used to tune device behavior and to enhance memristor performance. It is going to be divided in sections presented as following:

The first chapter provides an overall introduction to the work. The second chapter is the literature review of memristors and tantalum oxide-based memories. The idea is to explain the basics of memristors: types of memristors, switching mechanism, operation, design and electronic transport.

The third section covers the objectives of the proposed research project which is basically to develop and design a memory device with enhanced performance by engineering of defects: the idea is to promote oxygen vacancies by adding zirconium on tantalum oxide and also by controlling the oxygen atmosphere during deposition of the active layer using pulsed laser deposition (PLD).

The fourth section Methods, covers the preparation of the doped source (target) and characterization methods used to account the effect of doping on film surface by atomic force microscopy (AFM), the composition by x-rays photo electron spectroscopy (XPS), electronic structure by ellipsometry (SE) and transport characteristics through electrical measurements and modelling. Finally, device behavior by electrical parametrization.

In section fifth Results and Discussion, the effects of doping and change of pO_2 during deposition is explained. The electronic structure obtained by SE and composition results from XPS analysis suggest an increase in oxygen vacancy content due to Zr doping and deposition in low oxygen partial pressure atmosphere. These vacancies are represented as in-gap states and non-stoichiometric phases. The device behavior is further analyzed by electrical measurements and using hopping model the oxygen vacancy content was estimated. As it is going to be presented and discussed, Zr doped devices and devices prepared at low oxygen partial pressure conditions (Intrinsic doped) presented enhanced performance in terms of: cycle to cycle variability, resistance window, electroforming, analog behavior, etc.

2. Literature review

2.1. Resistive Switching

Resistive switching is a physical phenomenon observed in a capacitor-like stack of thin layers of dielectric materials (Oxides, chalcogenides, polymers, 2D materials, etc) submitted to high electric fields [1], [2]. It is basically the change of the resistance state of a dielectric thin layer induced by electric field. As a non-volatile multi-state device, it can be used as a computer memory that has the capability to hold and save data. This phenomenon has been studied since the middle of last century but it was set aside due to the discover and boom of the transistor silicon industry. Recently, in 2000's pushed by the memory density and scale limitation predicted by Moore law of the silicon-based transistors memory industry; computer industry started to target a novel technological option for memory application. Suddenly, the interest in resistive switching resurge accompanied by newly discover and first attempt to understand the resistive switching physical phenomena made by the research group headed by professor Stan Williams at HP labs [13]. They claimed that a titanium oxide based resistive switching device can be related to the fourth fundamental two terminal electronic component postulated by Prof. Leon Chua in 1972 at University of California Berkeley[14], figure 1.

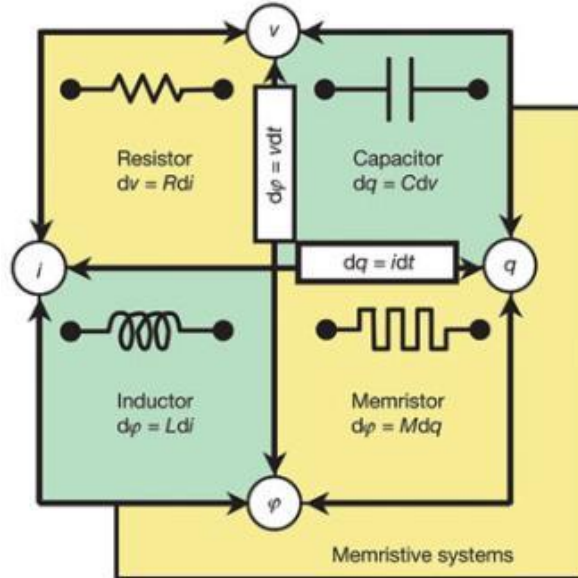


Figure 1: The fourth fundamental two terminal electronic components and its fundamental pair of variables. In the case of the memristor it is flux and charge. Figure taken from Ref.[13].

The memristor postulated by Leon Chua relates magnetic flux and the electric charge (See figure 1). According to Chua unlike resistor, memristance (M) which also relates voltage and current is not a constant but rather depends on a dynamical state variable which is the charge. Then, memristor resistance (memresistance) basically depends on the current passing through it over time. According to HP labs model the titanium oxide memristor resistance changes according to the ratio between the length of a low resistance doped region (non-stoichiometric titanium oxide) and the total length of the memristor active layer (dielectric layer). This doped region length can be modulated by electric field. For a more detailed explanation about the electronic and phenomenology explanation about memristor see ref [13], [15]. It turns out that the first phenomenological model presented by HP labs is not exactly accurate and eventually there is no experimental evidence of the actual relation between magnetic flux and the resistance (memresistance) still. Since then, lots of other devices are being made and different materials are also being used. Research groups and companies worldwide are investigating and studying this two-terminal device whose is being used as a new building block option for memory applications. Another important behavior besides its simple structure, small size and passivity that enable memory densification, and low power consumption, is that it also presents brain-like behavior for neuromorphic computing and then it is also enabling a possible novel and more rapidly computer architecture in oppose to Von Neumann architecture[16]. It should be noted that, in this work, resistive switching or ReRAM can be also referred to as memristors, both are interchangeably used.

2.2. Types of RS

There are basically three types of resistive switching[17]: phase change mechanism, electrochemical switching mechanism and valence change mechanism, see Figure 2. In the phase change mechanism (PCM), the dielectric active layer usually a chalcogenide material suffers phase change by joule heating: It is initially amorphous with a high resistance state (HRS), OFF state, and then become crystalline with low resistance state (LRS), ON state (See figure 2-a). It is a reversible phenomenon; with a rapid high voltage pulse and high current levels the active layer reaches its melting point and then it is quenched to the amorphous state, the HRS, or OFF state. With a more continuous and stable voltage pulse the material can recrystallize and switch to the LRS, ON state, as shown in figure 2-a. On the other hand, the electrochemical metallization memory (ECM)

is based on the oxidation of an active electrode such as Cu, Ag and Ni and its diffusion and drift through a dielectric layer (oxides, selenides, or sulfides) towards an inert electrode such as Pt, W, Au under high electric fields.

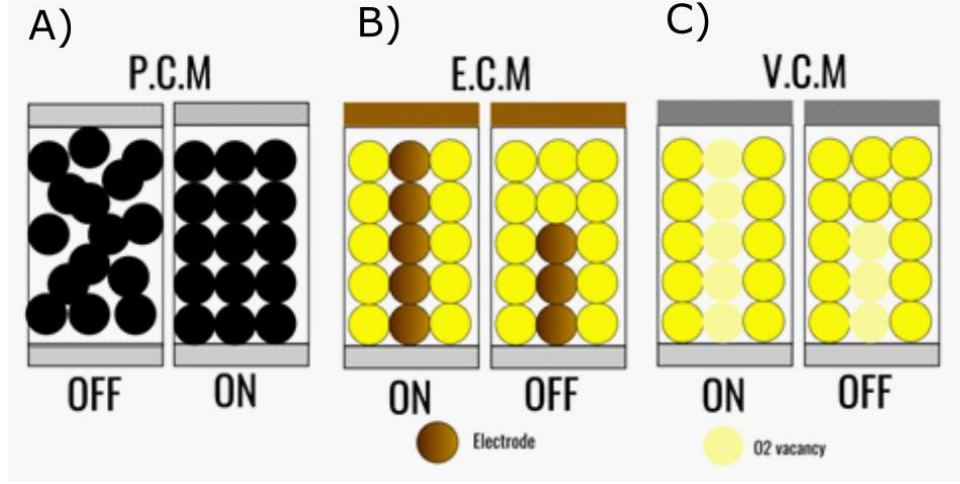


Figure 2: The well-known resistive switching types are a) phase change mechanism, b) electrochemical mechanism, c) valence change mechanism.

The electrode ions are reduced and form a conductive filament bridging both electrodes and then reducing the active layer resistance switching to LRS (see figure 2-b). Finally, the last one, which is dealt with in this work, the valence change mechanism (VCM) is based on the change of the valence of the cation of the metal oxide layer under high electric fields[18]. This leads to generation and movement of oxygen vacancies through the oxide layer towards the electrode forming a conductive filament or being evenly distributed through the oxide matrix decreasing its resistance, switching it to ON state (See figure 2-c).

2.3 Oxide based RS Devices: Valence change mechanism

Valence change memory resistive switching have been observed in binary and ternary metal-oxides such as TiO_2 , HfO_2 , SiO_2 , Ta_2O_5 , SrTiO_3 [1], [2], [7]. The mechanism behind this type of resistive switching material is the valence change mechanism. The explanation about how this happen is still under debate, but there are some strong evidences that the main element underlying the local resistance change is the oxygen vacancies. These oxygen vacancies are generated by joule heating, drift, and diffusion of oxygen ions (O^{2-}) toward the electrodes by the application of a voltage and this event is known as electroforming[18]. This makes a valence change of the metal in the metal-oxide layer.

During SET operation, these oxygen vacancies defects ($V_o^{\bullet\bullet}$ in Kröger–Vink notation) form a conductive filament bridging both electrodes and thus reducing the local resistance. During RESET, by applying an inverse polarity, O^{2-} hops towards these vacancy defects, the filament is dissolved and the resistance increase again [4]. $V_o^{\bullet\bullet}$ formation can also be induced prior to current application by depositing non-stoichiometric oxides (intrinsically doping) or even by doping the metal oxide with an aliovalent cation (extrinsically doping) with one less valence electron thus inducing O_2 evolution and $V_o^{\bullet\bullet}$ formation in order to keep electroneutrality[11], [19]. Devices with oxygen vacancies generated prior to current application sometimes happen to be forming free devices. When a sufficient $V_o^{\bullet\bullet}$ content is present, they already start with low resistance state and thus do not need a forming step to start operating.

The oxygen vacancies can be distributed in two different ways under application of a high electric field. One is by creating a nanometer scale conductive filament bridging both electrodes that can be formed and partially dissolved according to cycling (switching) polarity as depicted in figure (2-c). This device is then area independent once the filament has a size much smaller and independent of the electrode area. The other type of oxygen vacancy distribution can be uniformly distributed throughout the whole film and electrode area, changing resistance homogeneously over the film area. It is called homogeneous-type switching and it is area dependent. Both types of distribution can happen alone or simultaneously[20].

2.4. RS Devices Basic Operations types

There are basically three types of operations in resistive switching devices. The most common is the bipolar resistive switching (see fig. 3 (a)) [18]. To change the device resistance, it is necessary to apply a voltage higher than a threshold value, V_{th1} , also called minimum switching voltage. To switch it back to its past resistance state, it is necessary to apply an opposite polarity voltage with a different threshold value, V_{th2} . In the unipolar switching operation (see 3-b), the set and reset operation occur at the same voltage polarity and each one has a different switching voltage (Threshold voltage). To read the resistance value in both types, it is necessary to apply a voltage lower than the threshold one. The complementary resistive switching is operated above a threshold value V_{th1} and V_{th3} for each polarity, it must be read above this value, and can be switched (write) above

another threshold value V_{th2} and V_{th4} . The most common operation in tantalum oxide based memristors is bipolar switching.

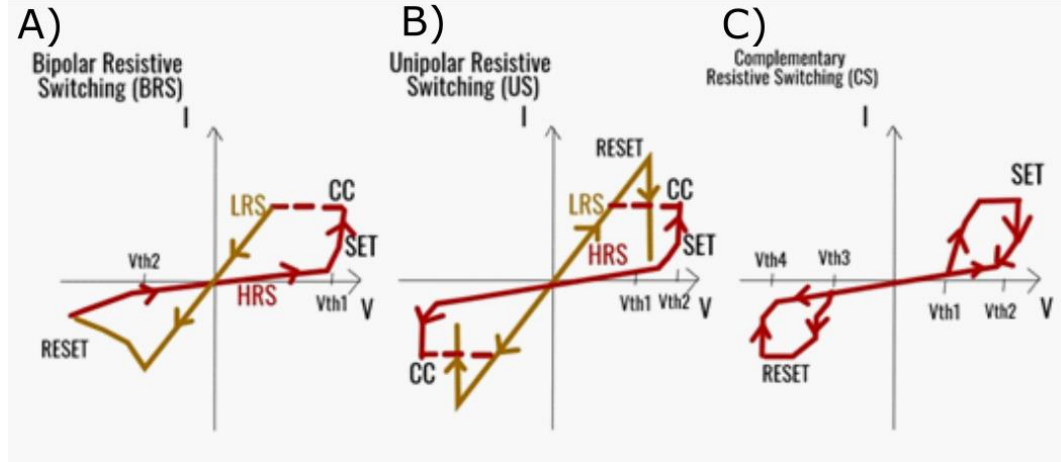


Figure 3: I-V characteristic curve (sweep test) of a typical a) Bipolar resistive switching device, b) Unipolar Resistive switching device and c) Complementary Resistive Switching device.

2.5. BRS Operation Parameters

Pristine devices usually start with a high resistance state since stoichiometric metal oxides are insulators. In order to operate the device, it must be initially submitted to a high electric field higher than the nominal voltage operations to switch it between LRS and HRS. It is called the electroforming step (forming voltage, $V_{forming}$), and it is well accepted that it is responsible for oxygen vacancy generation in VCM devices[18]. As it is going to be discussed in further sections, some devices can be doped in order to make them initially non-stoichiometric, oxygen vacancy rich[19][21]. These devices are forming free and initially operate in LRS or HRS without the need of this forming process. During forming and normal switching operation the current level must not surpass what is called the breakdown current which is responsible for an avalanche dielectric breakdown that irreversibly changes the device resistance to a short resistance state. Then, in order to keep device integrity, it must be operated with a compliance current (current compliance, CC) that limits the current level of operation.

Some studies are showing that as the first forming step is a stochastic phenomenon it does not guarantee a homogenous condition for different devices. This might be responsible for one of the most common problems faced by this technology implementation which is the fluctuation of the device operation parameters [22]. Thus, it

is of technological interest to study means to reduce this variability and doping is one of the options. The switching operation from LRS to HRS is referred as SET and the contrary operation as RESET, then there are the SET voltage (V_{set}) and RESET voltage (V_{res}).

Another important parameter for technological application is the resistance window or R_{on}/R_{off} which is the ratio of LRS by HRS. Normally as a convention, LRS and HRS are taken at a reading voltage between 0.2 V and 0.4 V once a voltage value higher than that could potentially change its resistance state.

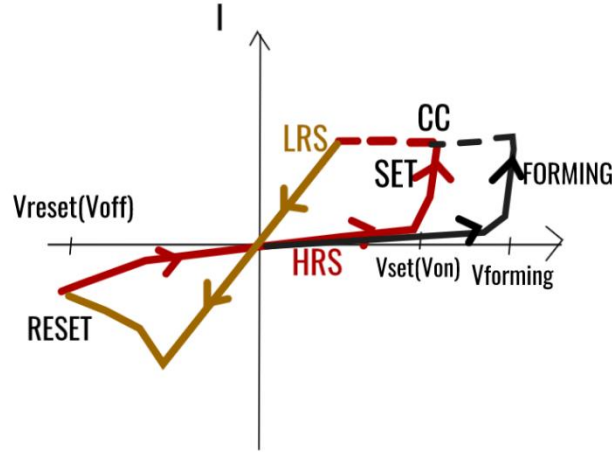


Figure 4: Typical I-V sweep curve of a RS device.

Retention time is the amount of time a memory device can maintain its resistance state, for that, a reading step is made time by time. Finally, endurance is the maximum number of switching cycles until it gets stuck in a low resistance value irreversibly (Breakdown). These parameters can be acquired in a DC static measurement I-V curve (sweep test) or in a pulsed measurement. In this work all device parameters are acquired by means of I-V sweep-test that will be further discussed in the section Methods Electrical parametrization.

2.6. Tantalum oxide-based RS Devices

Tantalum oxide based resistive switching devices presents the highest endurance ratio ($\sim 10^{12}$ Cycles) observed so far and high $R_{on}-R_{off}$ ratio. In addition, tantalum oxide films are used on current silicon memory application as high-K layers (BEOL systems) then they offer an advantage since they could be fabricated using current installed facilities[23], [24]. The Ta-O system presents only one stable oxide phase Ta_2O_5 ,

nonstoichiometric suboxides are metastable[25]. Normally tantalum oxide-based switching layers are typically amorphous or polycrystalline and normally nonstoichiometric in order to increase oxygen vacancy content and then reduce electroforming voltage set and reset voltages [21], [26]. Thus, the switching material is going to be referred sometimes as TaO_x . A study made on a TaO_x system by in situ high resolution transmission electron microscopy (HRTEM) and electron energy loss spectroscopy (EELS) has shown evidence that a conduction filament is formed and dissolved during set and reset operation, respectively[27]. According to this study, an amorphous sub-stoichiometric phase region of few nanometers is surrounded by a nanocrystalline Ta_2O_5 region. Quantum simulation studies of tantalum oxide structures reported the occurrence of metallic sub stoichiometric phases [27]. This suggests that TaO_x resistive switching devices are normally of VCM type. Ta_2O_5 switching layers are normally deposited by reactive sputtering, DC sputtering, atomic layer deposition and few studies by pulsed layer deposition.

2.7. Doping Effects on oxide-based ReRAM devices

DFT studies on dopant effects (extrinsic doping) for oxide based memristors such as HfO_2 , TiO_2 , ZrO_2 and Ta_2O_5 have shown that doping could provide higher switching uniformity, lower set voltage and reduce forming voltage due to enhanced oxygen vacancy formation [28], [29]. There have been also some studies investigating intrinsic doping effects on Ta_2O_5 showing that non-stoichiometric tantalum oxide promotes lower forming voltage and switching voltages. The intrinsic doping in thin tantalum oxide films occurs whenever the compound stoichiometry ratio deviates (oxygen deficient) without adding an external chemical specie and it takes place for radio frequency (RF) sputtering and pulsed laser deposition (PLD) by either controlling the oxygen partial pressure during thin film during growth [10], [26], or parameters such as the power of the RF source[21], the laser energy in PLD[30], or even the temperature during and after deposition process (annealing) [31]. On the other hand, extrinsic doping occurs when atoms of a foreign element are added to the compound. For instance, experimental investigations were done by co-sputtering two targets of SiO_2 and Ta_2O_5 [11]. Also, by atomic layer deposition (ALD), mixing ZrO and Ta_2O_5OH [12], and in PLD of cerium oxide (ceria) thin films using gadolinium doped ceria target[19]. According to reference [12], doping tantalum

oxide layer with 20% (mol) zirconia decreased the switching voltage and increased the $R_{\text{on}}-R_{\text{off}}$ ratio.

2.8. Bi-layered oxide-based ReRAM devices

It is worthwhile to mention that there are several recent studies on device engineering and design to investigate the influence of the electrode material and device stack combination of materials on device performance and applications. Recent works have been reporting novel methods to induce analog switching, multi-state and neuromorphic behavior in normally reported bi-state devices - see figure 5 to understand the difference between digital and non-abrupt switching (Analog) [6], [32], [33]. For instance, according to reference [34], single layer devices, i.e., devices with just one active layer (for example: Ti-HfO₂-Pt), normally display abrupt (digital) SET and RESET switching while bilayered devices, with an active layered composed of two different oxides for example Ti-TaO_x-HfO₂-Pt have a much more gradual SET/RESET process, which is also referred as analog switching. These devices normally present more than two resistance states which can be modulated by I-V pulsed cycling and then they could be used in bio-inspired neuromorphic applications. There are also other works studying bi-, triple or quadruple layered device stacks. These extra layer works as a reservoir of O⁻² or oxygen vacancies, or even can change oxygen diffusion dynamics and thus can change switching characteristics for different applications[17][35].

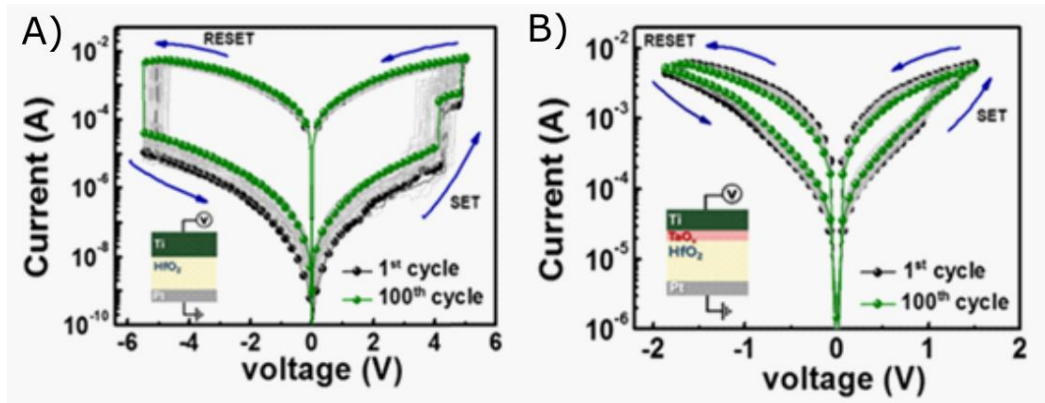


Figure 5: The bipolar characteristic after sweep cycles on a) Single layer and b) bi-layered ReRAM devices.[17]

2.9. Electronic transport in tantalum oxide-based ReRAM devices

Several charge transport mechanisms have been reported to explain electronic conduction in oxide films[36]. Electrons can be transported from one electrode to the other passing through the oxide layer in different ways. The conduction mechanism can be divided into: interface and bulk type mechanisms that occur simultaneously with each other. Thus, within a given voltage range, one usually prevails over the other and determines the measured electrical response. The transport mechanism will mostly depend on the electrode selection and the oxide characteristics. In tantalum oxide films, electrons can either jump from the electrode to the oxide conduction band, in what is called Schottky conduction mechanism (interface type) or they can go from one electrode to the other hopping through in-gap states, or charge traps, which in case can be oxygen vacancies (bulk type)[36]–[40]. In this case charges hop from one oxygen vacancy trap to the other (hopping conduction) or also by promoting an electron from these traps to the conduction band by decreasing the trap potential well with the electric field (Pole Frenkel). These models can be used to describe I - V dependence by means of analytical formulas using some parameters of the insulator. The best model used to describe the electronic transport is assumed to be the one that best fit and gives reasonable parameters for the tantalum oxide insulator.

For bilayer tantalum oxide devices according to reference [38], [41] for the initial voltage range electronic transport can be well described by hopping conduction. The current density can be ascribed as:

$$J = qanv \exp\left(\frac{qaE}{kT} - \frac{\phi_t}{kT}\right) \quad (1)$$

Where a denotes an average distance between trap sites, ϕ_t is the trap energy, k is Boltzmann constant, q is the electronic charge, n is the carrier concentration, v is the attempt-to-escape frequency and E is the electric field. By using the hopping model to adjust experimental I - V curves, the distance between traps (oxygen vacancies) and trap energy can be obtained.

3. Objectives

3.1. General Objectives

There are few studies about the effect of doping on tantalum oxide based memristors using transition metals oxides such as Ti, Zr, Hf, Al. Specially on using target alloying, there is no previous works on pulsed laser deposition (PLD)[42]. The main proposal of this work is to prepare, characterize and investigate the effect of intrinsically (oxygen partial pressure control) and extrinsically (Zr doping) doping on tantalum oxide based bi-layered resistive switching devices deposited by means of pulsed laser deposition aiming at engineering applications in neuromorphic computing and mass storage memory devices.

3.2. Specific objectives

- Preparation of pure tantalum oxide and mixed tantalum oxide and zirconia PLD targets.
- Deposition and characterization of the pure tantalum oxide thin film and of the Zr doped tantalum oxide.
- Study of the effect of doping on the defect content of the device active layer: electronic transport analysis, and thin film characterization.
- Device fabrication: micropatterning and deposition of electrodes and active layer.
- Electrical parametrization of the resistive switching device and analysis of doping effect on device performance.

4. Materials and methods

4.1. Target manufacturing

A NETZSCH DIL 402 PC dilatometer was used to investigate tantalum pentoxide (Optipure, Merck) sintering conditions. Dynamic and static temperature regimes were performed in order to find sintering time and temperature for the solid-state synthesis of the PLD targets. From the start, a tantalum pentoxide sample of rectangular section (20x4) mm² and 3 mm long was arranged for dilatometry test. The mass was determined considering green density of 3 g/cm³ and sample volume (matrix) of 240 mm³ (20x4x3). The pressure was determined assuming a force of 1 ton-F and an area section of 80 mm² (20x4). Then, 0.78 g of tantalum pentoxide powder was uniaxially pressed for 30 seconds through a hydraulic press machine using a stainless-steel matrix applying a pressure of 30 bars. A dynamic ramp was set and performed in a nitrogen rich atmosphere (125 ml/min; 1 bar) going from 25 °C to 1550 °C with heating and cooling rates of 10 °C/min. The densification temperature was acquired by taking the slope of the sample contraction ($(dl - \text{Current length}) / (dl_0 - \text{Initial length})$) by the temperature during dynamic test. A static ramp was done with a heating rate of 10 °C/min going from 25 °C up to 1400 °C which according to dynamic test has the greater densification rate. This temperature was then kept for 2 hours and then the sample was cooled down to 25 °C with a step of 10 °C/min. The density was measured and the sintering time for the target sample was determined extrapolating the curve in the static regime to reach the contraction needed to achieve a target relative densification of minimum 70% (For a tantalum oxide theoretical density of 8.2 g/cm³).

Pure Ta₂O₅ and ZrO₂ + Ta₂O₅ doped target with 25.4 mm in diameter and 4 mm thick were produced. The powder mass was estimated considering the target volume aforementioned and a green density of 3g/cm³. 4.5 g of Ta₂O₅ powder were then pressed in a stainless-steel matrix of circular section of 25.4 mm in diameter for 30 second applying a pressure of 200 mbar. For ZrO₂ + Ta₂O₅ target, a mixture of 20 % mol (0.3 g) of ZrO₂ and 80 % mol (4.2 g) of Ta₂O₅ – 3%atZr-Ta₂O₅ - were homogenously shaken for 15 minutes in a TURBULA shaker mixer model T2F and afterwards pressed same way as pure Ta₂O₅ target. Pure and doped targets were sintered for 5 and 8 hours, respectively. Reaching a densification of 65% both. X-rays diffraction patterns for both

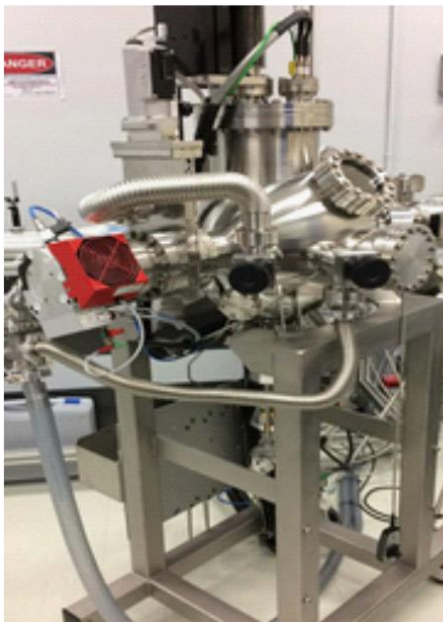
targets are in appendices section. As suggested by XRD analysis, Zr is solubilized in Ta_2O_5 in which in case forms an β - Ta_2O_5 (orthorhombic crystal system) - See more detailed information in appendix section.

4.2 Thin-Film preparation and characterization

4.2.1. Pulsed Laser Deposition

Tantalum oxide and zirconia mixed tantalum oxide thin films were deposited by means of pulsed laser deposition (PLD) using a 248 nm KrF excimer laser and a TSST vacuum system (see figure 6) (CCCH – IPEN, São Paulo). The zirconium doped tantalum oxide target mixture of 20% ZrO_2 (mol fraction) or 3at% of Zr was selected based on a previous work with atomic layer deposition [12] which displayed a better performance in terms of reliability for this mixture fraction. The laser energy used was 70 mJ with a spot size of 2.3 cm^2 , the repetition rate was 10 Hz and the set distance between target and substrate was 45 mm. Depositions were done at 25°C and oxygen partial pressure was varied from 5×10^{-3} mbar to 1×10^{-1} mbar in order to obtain non-stoichiometric films.

A)



B)



Figure 6: a) Pulsed Laser Deposition System, b) tantalum oxide based and mixed zirconia and tantalum oxide targets

4.2.2. Chemical characterization

In order to find out the stoichiometry of the oxide thin film prepared using different oxygen partial pressures, X-ray photoelectron spectroscopy (XPS) were done for the tantalum oxide thin films. XPS data refinement was made using Thermo Scientific™ Advantage (CEM-UFABC, Santo Andre, SP). Deconvolution and fitting were made using the “smart fitting” option. The binding energies considered in the fitting procedure for each oxidation state can be encountered in the appendix section.

4.2.3. Thin film Optical properties

Tantalum oxide Thin films deposited on silicon substrate with native oxide layer (20 nm) were analyzed through a J. A. Woollam M-2000 Ellipsometer, Variable angle spectroscopy ellipsometry (VASE), covering wavelengths from 193-1690 nm and angles of 45°, 55° and 65° (Physics department, UFMG, Belo Horizonte, MG). The Tauc-Lorentz model were used to fit the ellipsometry spectra and then optical constants, absorption coefficient, thin film thickness and roughness of the active layer were acquired.

4.2.4. Thin film surface topography

Surface topography of thin films was acquired using a Bruker MultiMode8 HR (CCTM-IPEN, São Paulo) on PeakForce Tapping mode, the acquisition was done over 1 μm^2 and 0.25 μm^2 areas. SEM image was also acquired using a FESEM JEOL JSM-6701F (CEM-UFABC, Santo Andre, SP).

4.3. Thin-film Preparation of the Resistive Switching Devices

In order to evaluate the effect of oxygen partial pressure (intrinsic doping) and Zirconium doping (extrinsic doping) on device performance, two different combination of films were used to compare and study the effect of doping. Figure 7 shows a schematic drawing of the device configurations. Two types of stacks structures were investigated. For comparison, for each structure, we have produced devices with either pure tantalum oxide

layers or Zr-doped layers. The idea was to compare the effect of Zr doping with no contribution of a low oxygen partial pressure in device reduction and change in stoichiometry in structure type I, so active layer was prepared at a high $pO_2 = 1 \times 10^{-1}$ mbar - Ia is referred to Zr doped and Ib is referred to pure Tantalum oxide based. And the other idea is to analyze the effect of intrinsic doping, which is the effect of low oxygen partial pressure atmosphere in film stoichiometry and oxygen vacancy content, so both devices referred as structure type IIa (Zr doped) and IIb (Pure Ta based) are prepared in a relative lower oxygen partial pressure of $pO_2 = 2 \times 10^{-2}$ mbar.

The structure stack details are summarized in table 1 showing the pO_2 used and thickness in parentheses, and the devices are represented in figure 7. The PLD parameters used to deposit the active layer is the same for all structures: laser energy of 70 mJ, laser spot area of 2.3 mm^2 , repetition rate of 10 Hz and temperature of 25°C . The only parameters that was changed for the different proposed structures are the pO_2 and the target (Zr:Ta₂O₅ and Ta₂O₅ based).

In structure type I, which is a similar structure as the one used in reference [35], a relatively thick (40-80 nm) non-stoichiometric Ta₂O_x layer (Ib) or Zr:Ta₂O_x (Ia), deposited at low oxygen pressure $pO_2 = 5 \times 10^{-3}$ mbar, is used as an V_o^- source. A thinner (12-14 nm) layer, deposited at oxygen rich atmosphere ($pO_2 = 1 \times 10^{-1}$ mbar) that yields a close to stoichiometric Ta₂O₅ (Ib) and Zr:Ta₂O_x (Ia) composition, is used as the active layer where switching preferably occurs (dissolution and formation of conductive filament)[18], [35]. It is reasonable to assume that switching behavior of device type I is mainly controlled by the characteristics of the more insulating top layer, as its oxygen content is close to stoichiometry, in which most part of voltage drop occurs across this layer. The bottom layer prepared is more conductive as compared to the “oxygen stoichiometric” layer and thus act as a vacancy reservoir layer [35].

In type II devices, an active 10 nm-thick layer is prepared with an intermediate oxygen pressure ($pO_2 = 2 \times 10^{-2}$ mbar) and capped with a very thin passivation layer (<1nm) deposited at $pO_2 = 10^{-1}$ mbar. For type II devices, the critical layer for the initialization and switching is the one prepared at 2×10^{-2} mbar, the cap layer is used for passivation of surface defects and should not play a role in the switching behavior.

In summary, type I devices have active (switching) layers deposited at high oxygen pressure ($pO_2 = 1 \times 10^{-1}$ mbar) that have a relatively lower vacancy concentration, whereas type II devices have active layers deposited at an intermediate oxygen pressure ($pO_2 = 2 \times 10^{-2}$ mbar) that have a higher concentration of V_o^- .

Table 1: Device stack description of structures type I and II. pO_2 used to deposit the oxide and thickness are represented in parenthesis.

	Bot electrode	Active layer	Top electrode	
Ia	W (60)	Zr:Ta ₂ O ₅ (40) $pO_2=5 \times 10^{-3}$ mbar	Zr:Ta ₂ O ₅ (15) $pO_2=1 \times 10^{-1}$ mbar	W (60)
Ib	W (60)	Ta ₂ O ₅ (80) $pO_2=5 \times 10^{-3}$ mbar	Ta ₂ O ₅ (15) $pO_2=1 \times 10^{-1}$ mbar	W (60)
IIa	W (60)	Zr:Ta ₂ O ₅ (10) $pO_2=2 \times 10^{-2}$ mbar	Ta ₂ O ₅ (<1) $pO_2=1 \times 10^{-1}$ mbar	W (60)
IIb	W (60)	Ta ₂ O ₅ (10) $pO_2=2 \times 10^{-2}$ mbar	Ta ₂ O ₅ (<1) $pO_2=1 \times 10^{-1}$ mbar	W (60)

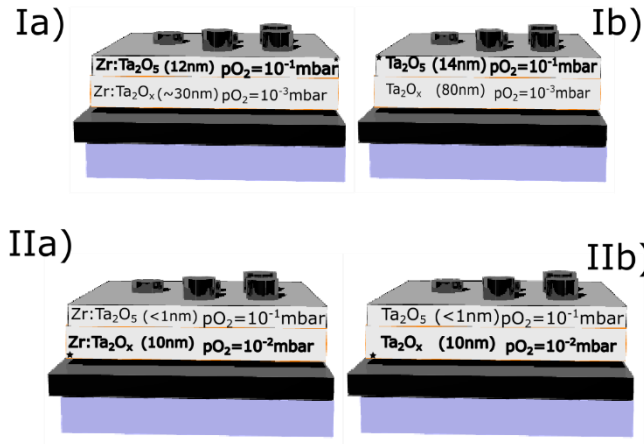


Figure 7: Structure stacks I and II. For structure type I the main layer is deposited at low oxygen pressure pO_2 ($pO_2 = 5 \times 10^{-3}$ mbar) and is used as an oxygen vacancy source. A thinner (12-14 nm) layer, deposited at oxygen rich atmosphere that yields a close to stoichiometric Ta₂O₅ composition. In the devices with structure type II, an active 10 nm-thick layer is prepared with an intermediate oxygen pressure ($pO_2=2 \times 10^{-2}$ mbar) and capped with very thin passivation layer (<1nm) deposited at $pO_2=1 \times 10^{-1}$ mbar.

4.4. RS Device micro-fabrication process

The device stacking fabrication process is shown in figure 8 for a dot pad type device (common bot) and cross-point type device (“dog-bone”) [22]. Starting from a silicon substrate with a silicon oxide layer of 285 nm in fig 8a) and 8d), a RF sputtered tungsten bottom electrode was deposited; The substrates were cleaned in ultrasonic baths for 5 minutes each in distilled water, ethanol and acetone. Tungsten bottom and top electrodes were deposited by RF magnetron sputtering system (ATC Orion Series) (Physics department, UFMG, Belo Horizonte, MG). accommodating a high-purity 99.98%

tungsten (W) target. The deposition parameters were the following: plasma power of 200 W, pressure of 8 mTorr, argonium flow of 10 cm³/min and temperature of 25°C. As shown in figure 8b and 8e, over tungsten bottom electrode, tantalum oxide film was deposited (the pure and the Zr doped target) by PLD – see table in the previous section for more detailed description of the oxide structure type I and II used in this work as the memristor active layer. Finally, the tungsten top electrode of the metal-insulator-metal (MIM) memristor structure was RF sputtered (See fig. 8c).

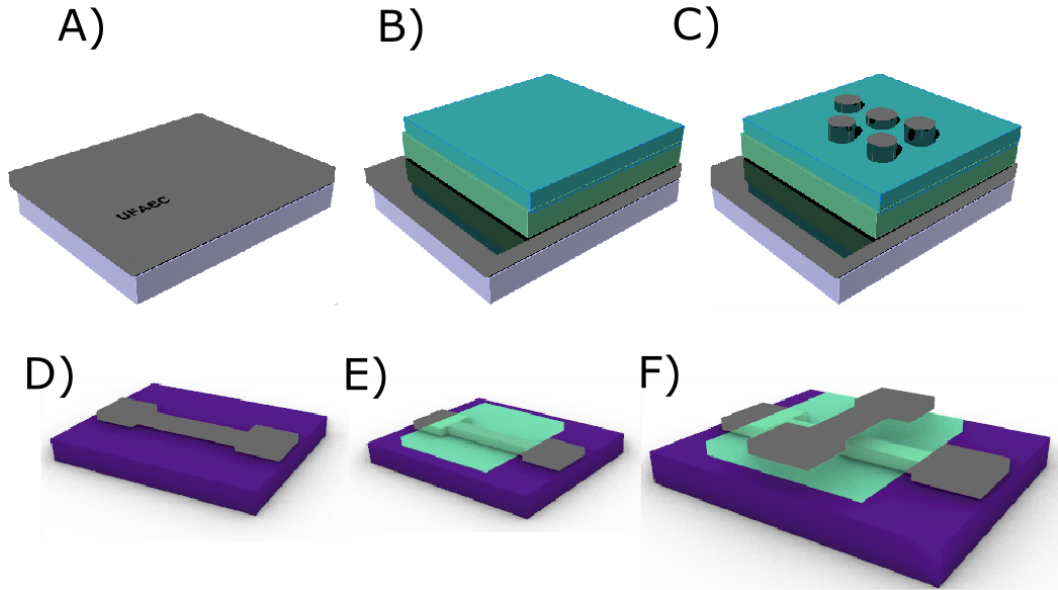


Figure 8: Device stack schematic of dot pad type devices (a-c) and cross-point (d-f) devices: (a) silicon substrate; (b) tungsten bottom electrode (BE); layered oxygen poor and oxygen rich tantalum oxide (for the pure and the ZrO₂ doped target) memristive cell; (c) micropatterned tungsten top electrode (TE). d) micropatterned tungsten bottom electrode, e) memristive oxide bilayer and f) micropatterned top electrode.

For a simple dot pad type device structure, represented in fig 8a) to 8c), the top electrode was proposed comprehending just one photolithography step. It was designed using CleWin 4.0 software and the patterns leads to four different rounded electrodes sizes. The size was chosen based on device pristine resistance and the probe-station tip landing limitation, which in this case are able to approach pads down to 80 µm in diameter.

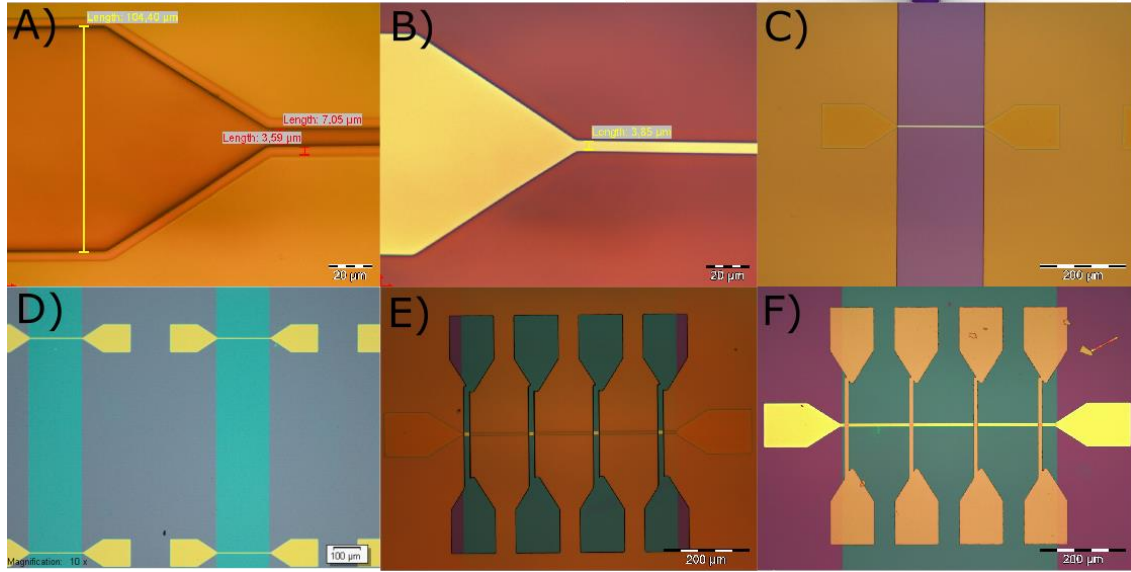


Figure 9: Cross-point device fabrication schematics: (a) After developing photoresist mask bottom electrode, followed by (b) deposition of tungsten and afterwards lift-off process. Right after, (c)(d) another mask was also prepared for PLD deposited oxide active layer. After that, (e)(f) photoresist mask for top electrode were also prepared over both bottom and active layer to deposit tungsten top electrode.

The cross-point type structures showed in detail in figure 9 were prepared to achieve smaller area devices ($\sim 3\mu\text{m} \times \sim 3\mu\text{m}$). They were prepared in three micropatterning steps, one for bottom electrode (fig. 9a), followed by deposition of tungsten and afterwards lift-off process (fig. 9b). Right after, another mask was also prepared for PLD deposited oxide active layer (fig. 9c and 9d). After that another photoresist mask on top of both bottom and active layer were finally prepared to deposit tungsten top electrode (fig. 9e and 9f). Photolithography was performed in a class 100 cleanroom facility using a Microtech Laserwriter model LW405 (Physics department, UFMG), figure 10. The spinner speed was 4000 rpm for 5 s and the acceleration was 1000 rpm.s^{-1} then the second spinning round was done with speed of 4500 rpm for 30s and acceleration of 2000 rpm.s^{-1} . The cure temperature was 115°C for 1 minute.

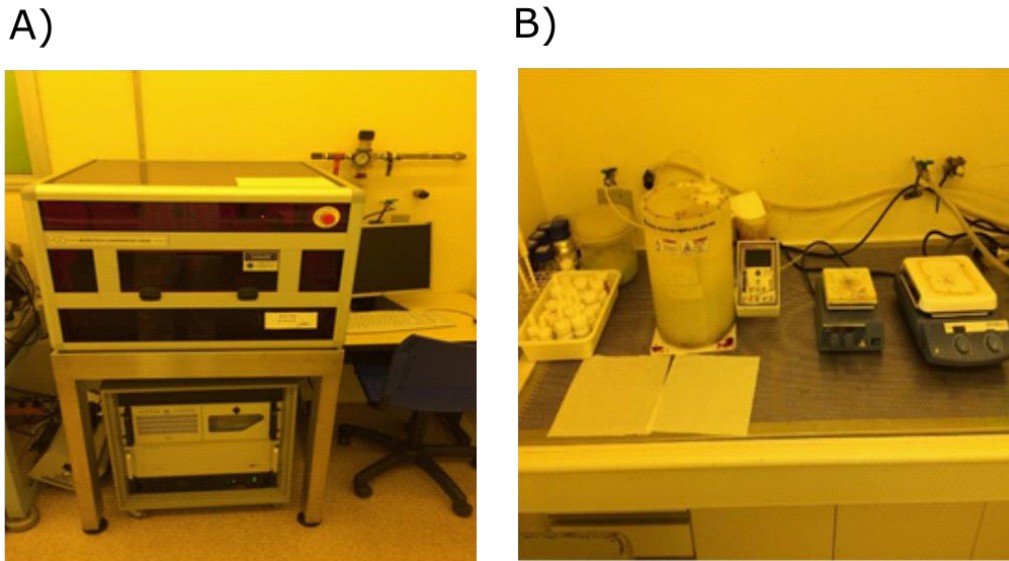


Figure 10: Clean room facility for micropatterning of the photoresist mask: a) Microtech Laserwriter model LW405 b) Spinner Laurell model WS-650SZ.

Photolithography was done with 10% filter, a gain of 150 and step 3 – these are specific parameters related to for the Microtech Laserwriter model LW405 software. The positive photoresist Microposit TM S1813 was deposited using a Spinner Laurell model WS-650SZ and developed using MICROPOSITTM MF26. Rounded top electrodes were micropatterned comprehending the following diameters 80, 100, 200 and 250 μm for dot devices and around 3 μm x 3 μm top and bottom cross-point devices.

4.5 Device Electrical parametrization

Devices were tested using a Wentworth Labs probe-station (UFMG and UDES), figure 11. Current–voltage (I-V) testing of these devices was done using the Keysight B1500A Semiconductor Device Parameter Analyzer (OPTMA lab, electrical engineering department, UFMG) and the Keithley 4200A-SCS Parameter Analyzer (LCSM - 3IT center Université de Sherbrooke, Sherbrooke, QC, CA).

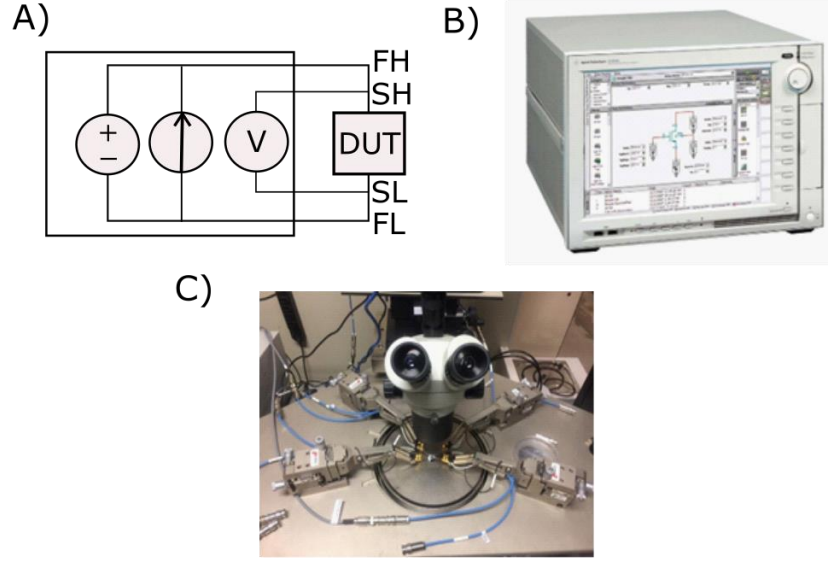


Figure 11: Device parametrization and testing using a a) 4 probe westwood probestation b) keysight B1500 and a c) Device under test (DUT) testing setup scheme with two source meter units (SMUs) for voltage and current measurement (Sense High, Sense Low) and voltage application (Force High, Force Low)

The device test routine used was a DC voltage or current sweep. The device characteristic curve was performed with writing and reading cycles from 0 V to set or reset voltage values (1 – 4 V) with a step voltage ranging from 2mV to 20mV. All ON and OFF resistance states referred in this work is at a reading voltage of 0.2 V.

4.6 Electronic transport analysis

Electronic transport studies were carried out in pristine devices prior to electroforming. As suggested by previous works [19], [29] extrinsic and intrinsic doping can enhance oxygen vacancy content [19], [42]–[46]. To account it, the hopping conduction model was adopted to analyze the I - V curves of the devices. In this model, electronic transport is dominated by electron hopping between trap sites that are formed due to the presence of oxygen vacancies. [36] The current density can be ascribed as:

$$J = qanv \exp\left(\frac{qaE}{KT} - \frac{\phi_t}{KT}\right)$$

Where a denotes an average distance between trap sites, ϕ_t is the trap energy, K is Boltzmann constant, q is the electronic charge, n is the carrier concentration and ν is attempt to escape frequency. This model was implemented to fit all IxV curves of pristine devices using a python script, `scipy.optimize` and `curve_fit` libraries were used.

5. Results and discussions

In this study, the influence of oxygen non-stoichiometry and of Zirconium doping on the resistive switching performance of tantalum oxide based memristive devices was investigated. First, surface analysis was carried out by AFM and SEM. It was performed to investigate and study the surface aspect and eventual changes induced by different pO_2 used during deposition and Zr addition. Surface roughness becomes important once active layer interface plays a vital role on device functioning. The roughness can change the electric field distribution over the active layer and can also induce localized conductive channel formation. Finally, it's almost intuitive that roughness can change the device active layer thickness and thus increase device to device variability[47].

XPS analysis was carried out to find the change in the oxide stoichiometry by depositing it in an oxygen poor atmosphere. As it was shown in introduction section, tantalum oxide stoichiometry plays an important role in switching once it can change the local conductivity accommodating oxygen vacancies. Intuitively, deposition of oxide in an oxygen poor atmosphere leads to sub-stoichiometric films with less oxygen on its structures and more oxygen vacancies [45], [48]. So naturally, tantalum oxide films prepared at oxygen poor conduction should be identified in XPS spectra with a huge contribution of non-stoichiometric phases (Ta^{4+} , Ta^{3+} , Ta^{2+} , Ta^{1+} , Ta) which in case accommodate oxygen vacancies. High resolution scan of Ta4f peak of a film prepared at oxygen poor atmosphere was analyzed. Its Ta4f peak and survey scan was quantized and as predicted it is non-stoichiometric.

Same way, doping with an aliovalent cation, in this case ZrO_2 , can also change oxide stoichiometry and thus oxygen vacancy content. Charge imbalance generated by Zr^{4+} substitution of Ta^{5+} will induce O_2 promotion and thus V_o^- generation [29], [42], [49]. Thus, in order to investigate this, as predicted theoretically, oxygen vacancy can be noticed as in-gap state in the electronic structure of tantalum oxide [43], [44], [50]–[52] and ellipsometry spectroscopy analysis was performed to obtain the projection of the absorption spectra after modelling of the optical response (reflection acquisition). The increase in absorption intensity in a specific energy range can be attributed to the increase in oxygen vacancy content, so absorption spectra of films deposited at different oxygen partial pressure conditions and doped with zirconia were compared.

Another way to account the oxygen vacancy content is by electrical measurements, as oxygen vacancy can be considered as charge traps it plays a role in electronic conduction and changes the local conductivity, electronic models can be used to predict the amount of vacancies generated by the proposed methods (changing in oxygen partial pressure and Zr doping) [37], [38], [44], [52], [53]. So, films prepared in different oxygen partial pressure conditions and doped with Zr are compared as well. Thanks to hopping model, the oxygen vacancy content was estimate.

Finally, after noticing that Zr doping and low oxygen partial pressure deposition can contribute to increase of oxygen vacancy content, the devices were prepared and tested. The performance was analyzed by different memristor operation metrics, such as electroforming voltage which as previously discussed can influence in device operation variability and can increase cost due to operation complexity, etc [45]. Device electroformation in stoichiometric oxides are done in high voltage regimes and it is responsible for the oxide dissolution and formation of vacancy defects, which in case will form the memristor conductive filament. Thanks to the thermal contribution and high electric field promoted by its high voltage initial operation (electroforming) [39], [54]. As earlier observed [42], [45], [48], [55], [56], devices can start with defects (oxygen vacancies) and thus skip forming process. This strategy can be used to reduce variability once electroformation is a less controllable way to promote the oxygen vacancy formation.

Resistance window (ratio between high resistant state to low resistant state) was studied as well. It is an important parameter to take into account as it can also leads to increase in operation cost due to misreading of resistant state. Thus, higher ratios imply distinction between ON (LRS) and OFF (HRS) states and thus less cost in conditioning operations [22].

Finally, cycle to cycle variability was studied. It is an important characteristic, since device response should be predictable otherwise its application should be compromised. Thanks to the high randomness in formation and dissolution of the oxygen vacancy conductive filament [45], [55], [57]. As such, it was earlier shown in other works that dopants can interact with oxygen vacancies and confine the filament and thus decrease randomness and cycle to cycle variability [58], [59].

5.1 Thin film surface

As previous discussed, thin film surface play an important role in device functioning. The roughness can change the device active layer effective thickness and thus increase device to device variability. So, it should not have a rough surface otherwise it could be shortened or with a lot of functioning variation. The AFM analysis of a projected surface area of $0.25 \mu\text{m}^2$ indicates that the thin films are very smooth, see figure 12. For the thin films prepared using the mixed tantalum oxide and zirconia target and oxygen partial pressure of 5×10^{-3} mbar, 2×10^{-2} mbar and 1×10^{-1} mbar, the maximum roughness and mean roughness are indicated in Table 2:

Table 2: The AFM analysis of a projected surface area of $(0.5 \times 0.5) \mu\text{m}^2$ of the pure and mixed tantalum oxide thin films.

Target	Oxygen Partial pressure (pO ₂)	Mean roughness (Ra)	Max. roughness (Ra)
ZrTa ₂ O ₅	5×10^{-3} mbar	0.126 nm	1.270 nm
ZrTa ₂ O ₅	2×10^{-2} mbar	0.107 nm	0.810 nm
ZrTa ₂ O ₅	1×10^{-1} mbar	0.150 nm	1.400 nm
Ta ₂ O ₅	1×10^{-1} mbar	0.428 nm	4.240 nm

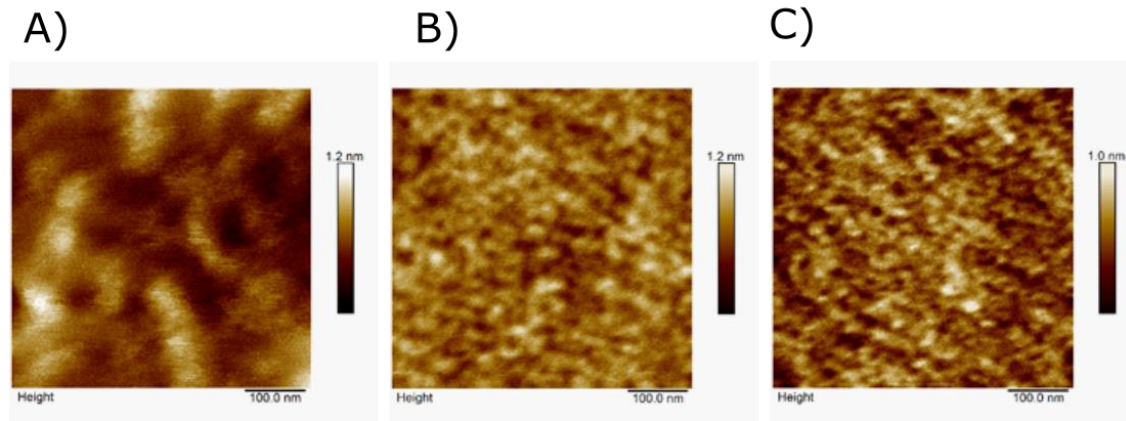


Figure 12: AFM analysis of the Zr doped Tantalum oxide thin films prepared with oxygen partial pressure of a) 0.003, b) 0.020 and c) 0.100 mbar.

In the same way, a pure tantalum oxide thin film prepared with oxygen partial pressure of 1×10^{-1} mbar was analyzed and according to AFM analysis it seems rougher.

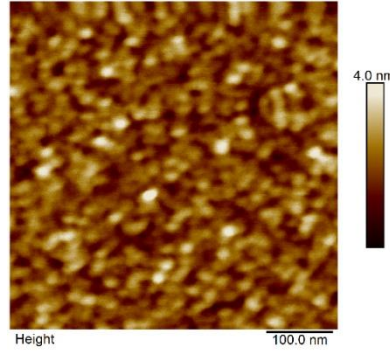


Figure 13:AFM analysis of the Tantalum oxide thin film prepared with oxygen partial pressure of 1×10^{-1} mbar.

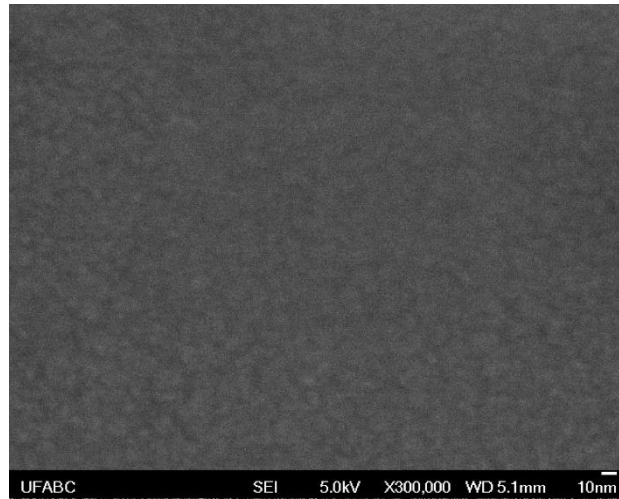


Figure 14:SEM image of the pure tantalum oxide thin film prepared at 1×10^{-1} mbar

The device roughness is in accordance with previous works [10], [47]. Scanning electron microscopy (SEM) image of tantalum oxide thin film prepared at 1×10^{-1} mbar also demonstrate that the film consists of a smooth and featureless layer, probably due to its amorphous nature, see figure 14. According to surface analysis, regarding surface characteristic, PLD deposition seems to present no limitation for memristor application.

5.2 Chemical analysis

A thin film prepared using the pure Ta_2O_5 target and oxygen partial pressure (pO_2) of 5×10^{-3} mbar was analyzed by XPS in order to account the effect of oxygen poor atmosphere on tantalum oxide composition. As the depth of interaction volume is of near 10 nm thick, in order to get rid of the native oxide layer, the measurement was taken after

surface ion-etching (argonium) of 30 seconds. High resolution scan of Ta4f peak of a film prepared at oxygen poor atmosphere was analyzed. Quantization of survey scan gives a non-stoichiometric O/Ta relation of 2.38 while a stoichiometric composition of Ta₂O₅ should give an O/Ta relation of 2.5 (see table 3). As earlier discussed, oxygen poor atmosphere can indeed induce non-stoichiometric composition [10], [48].

Quantization of high-resolution scan of Ta4f peak was performed to account the contribution of sub-stoichiometric phases to the oxide composition. These non-stoichiometric phases and thus contributions from Ta⁴⁺, Ta³⁺, Ta²⁺, Ta¹⁺ and Ta⁰ (representing TaO₂, Ta₂O₃, TaO, Ta₂O, and Ta metal, respectively) doublet peaks can be attested by deconvolution of the Ta4f peak [10]. These phases can play a role in local conductivity and also in oxygen vacancy accommodation. Previous scanning transmission electron microscopy studies and theoretical calculations of the electronic band structure of such metastable phases (TaO and TaO₂) have shown that they correspond to conductive phases that might leads to the formation of the conductive path during resistive switching to increase in local conductivity[27]. Reference [48] claims that Ta⁴⁺ oxidation state could be related to a good memristor performance once devices rich on theses phases presented more stabilized switching, better endurance and resistance window.

Deconvolution and quantification were carried out in XPS Advantage software, Ta4f doublet peak (Ta4f 7/2 and Ta4f 5/2) with energies corresponding to Ta⁵⁺, Ta⁴⁺, Ta³⁺, Ta²⁺, Ta¹⁺ and Ta⁰ oxidation states (representing Ta₂O₅, TaO₂, Ta₂O₃, TaO, Ta₂O, and Ta metal, respectively) used in this fitting procedure are presented in appendices section. The contribution from the more metallic phase is in around 22 eV range while the contribution from the more stoichiometric phase comes from peaks at around 29 eV.

As expected for this oxygen partial pressure condition used to intentionally prepare this sub-stoichiometric tantalum oxide film, the sub-stoichiometric composition of this film presents a content of more than 14% coming from Ta¹⁺, Ta²⁺, Ta³⁺ and Ta⁴⁺ sub-stoichiometric tantalum oxidation states and 0.26% of pure tantalum metallic. This can be understood as an increase in oxygen vacancy content.

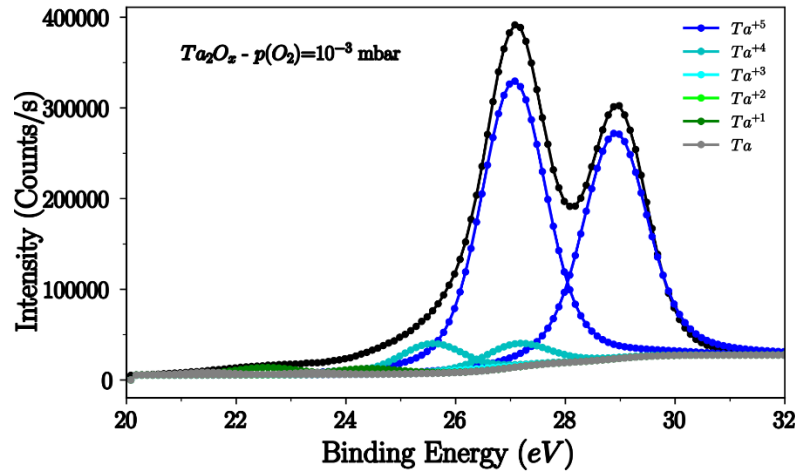


Figure 15: XPS analysis of the sample prepared using a pure tantalum oxide target and pressure of 5×10^{-3} mbar after 30 seconds of plasma etching.

In sum, according to XPS analysis of thin films prepared in pO_2 atmosphere of 5×10^{-3} mbar (oxygen poor atmosphere - intrinsic doped films), it is possible to promote the formation of non-stoichiometric tantalum oxide phases which can accommodate oxygen vacancies and leads to change in memristor behavior.

Table 3: The oxidation state and respective phase content for the sample etched for 30 seconds. The XPS survey analysis with the ratio of oxygen and tantalum for the Ta_2O_5 thin film.

Etch. time	Oxidation state					Survey	
	Ta(%)	Ta ¹⁺ (%)	Ta ²⁺ (%)	Ta ³⁺ (%)	Ta ⁴⁺ (%)	Ta ⁺ (%)	O/Ta
30''	0.26	0.57	1	2.19	9.02	86.93	2.38

5.3 Thin film Optical properties

Thin film optical analysis was carried out to study the effect of oxygen partial pressure and Zr doping effect on film optical properties and electronic structure. The optical response of oxide prepared in different oxygen partial pressure conditions and doped with Zr was taken in a reflection setup using three different angles as earlier discussed in methods. The optical response is given as a change in the optical signal polarization due to the interaction with the thin film and it is given as Psi and Delta parameters. Its response changes are given by a transformation matrix which take into account the material optical properties [60]. The model used to fit the psi and delta parameters over the entire spectral range from 1.7 to 0.3 μm were the Tauc-Lorentz [61].

After fitting the psi and delta spectra using the Tauc-Lorentz model, the oxide layer absorption spectra were obtained. As can be seen in figure 16 (a) and (b), thin films deposited at high oxygen partial pressure ($pO_2=1 \times 10^{-1}$) mbar have spectra typical of an insulator. They present an onset of absorption that is associated to the band gap at ~ 4.5 eV and have a negligible absorption in the sub gap region (i.e for photon energy below the band gap). Thin films prepared with oxygen partial pressure of 5×10^{-3} mbar and 2×10^{-2} mbar also have an onset of absorption at ~ 4.4 eV but present a broad absorption feature in the sub gap region. Such feature can be ascribed to oxygen deficiency, i.e. non-stoichiometry [43], [51], [62],[43], [62], [63].

Figure 16(c) presents the same results in a logarithmic scale. It allows a careful inspection of the sub-gap region of the films deposited at high oxygen partial pressure. For the pure tantalum oxide films, no sub-gap states are indeed detected. However, the spectrum of the Zr doped film presents a weak but non-zero absorption below the gap states which is an indication that Zr doping can indeed promote oxygen vacancy formation.

Here it is worth to emphasize, a limitation of this type of measurement, which is in a reflection mode and thus does not provide precise determination of weak absorption features. Further measurements of thicker films in transmission mode should provide a better description of such sub-gap states but are outside the scope of this dissertation.

The ellipsometry analysis also provided the thickness of the films and thus their growth rates as shown in table 4.

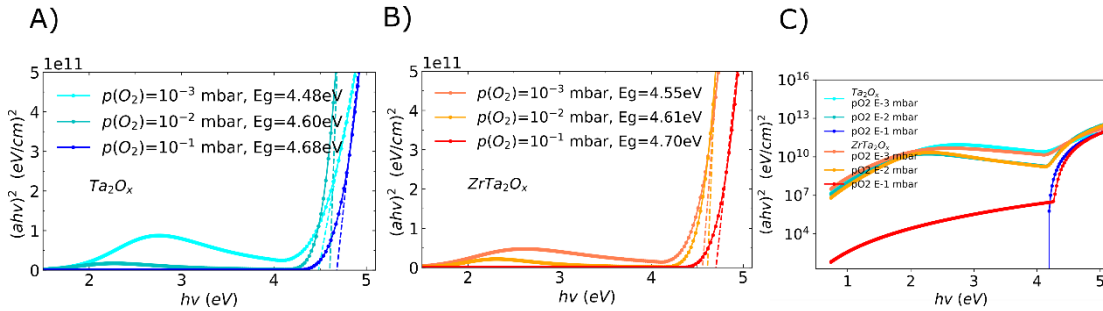


Figure 16: Absorption spectra of pure tantalum oxide and Zr doped tantalum oxide thin films prepared at oxygen rich and poor atmosphere pressure.

Optical band gap where also extracted from an extrapolation of the last linear portion of Tauc-plot which intercepts energy axis. Optical band gap goes from 4.48, 4.60, 4.68 and 4.55, 4.61, 4.70 to Ta_2O_x and $Zr:Ta_2O_5$, respectively for three different oxygen partial pressure: 1×10^{-1} , 2×10^{-2} , 5×10^{-3} mbar. It is possible to observe a narrow increase in gap energy due to Zr doping and a decrease in gap energy by decreasing oxygen partial

pressure. This change can be certainly attributed to doping but as previous discussed and proposed, a further study is needed to attest that. It should be carried out in a SE transmission setup rather than reflection, as it is more sensitivity and more proper used to evaluate optical absorption.

In sum, thanks to SE analysis we can provide a clear evidence of the effect of oxygen partial pressure on increase of oxygen vacancy content ascribed to the increase in absorption intensity of in-gap states associated to it. Likewise, Zr doping effect was also considered to increase the oxygen vacancy content as even films prepared at oxygen rich atmosphere happens to show non-zero absorption in the sub-gap region.

Table 4: Tantalum oxide and zirconium doped tantalum oxide thin film growth rate for different oxygen partial pressure conditions

	Thin film growth rate (nm.min ⁻¹)		
	pO ₂ = 5x10 ⁻³ mbar	pO ₂ = 2x10 ⁻² mbar	pO ₂ = 10 ⁻¹ mbar
ZrTaOx	0.96 nm.min ⁻¹	0.63 nm.min ⁻¹	0.43 nm.min ⁻¹
TaOx	1.30 nm.min ⁻¹	0.74 nm.min ⁻¹	0.61 nm.min ⁻¹

5.4. Device electrical parametrization

Quasi static DC characterization of memory devices are performed in order to obtain operation parameters. In this measurements, positive and negative cycling, operation going from origin to a switching voltage value, gives rise to the characteristic “pinched off” hysteresis loop, as previous shown in literature review section. The two resistance values considered for the switching memory are taken at 0.2 V, and it is called reading operation.

For all measurements, the bottom electrode is grounded. So, positive or negative voltages are applied to top electrode. Statistical analysis was taken out of around 10 resistive switching cycles for each device and respective device structure. As previous discussed in the methods section, for comparison, for each architecture, we have produced devices with either pure tantalum oxide layers (identified as structure Ib and IIb) or Zr-doped layers (identified as structure Ia and IIa). It is reasonable to assume that switching behavior of device type I is mainly controlled by the characteristics of the more insulating top layer deposited at pO₂=1x10⁻¹ mbar. So, for structure type I, it is going to be referred as the one prepared at oxygen rich atmosphere. For type II devices, the critical layer for

the initialization and switching behavior was prepared at 2×10^{-2} mbar, thus structure type II is going to be referred as the one prepared at oxygen poor atmosphere.

As previous discussed, device metrics analyzed here are: resistance window (HRS/LRS), forming voltage and cycle to cycle variability. These are all presented and discussed in the further sections.

5.4.1 Switching characteristics of type I devices

The devices tested have different pad sizes with diameters of 80 μm and 100 μm . In this section, for the sake of simplicity, just the results of devices with 80 μm are presented. The results for 100 μm (diameter) pads devices are in appendices section.

The first testing procedure is the electroforming step. The device normally starts with a high resistance value, which higher than resistance operations values of HRS and LRS, and a sufficiently high electric field must be applied to form conductive filaments. In our devices, such electric fields are generated by applying a negative voltage. As the bias voltage magnitude is increased there is a threshold value in which there occurs an abrupt change in the $I \times V$ curve. This behavior is depicted in Figure 17. The blue lines correspond to 2 different pure tantalum oxide devices with structure type Ib. They have an initial high resistance value, and in this case, the forming voltages were around -7 and -15 V.

Similar behavior was observed for some of the Zr-doped devices (type Ia), as depicted by the dark red line, even though the forming voltage was typically lower in magnitude. Surprisingly, some Zr doped devices start with a resistance value much lower, close to the switching HRS and LRS values. This is reflected in the higher slope in the $I \times V$ curve (red line). This is a characteristic of a forming free, or forming less device, which does not require high voltage electroforming step to start operating in the switching mode. This is an advantageous feature since as previous discussed, forming step can require high voltages and for large memory cross-bar matrix can be very time consuming and costly. So, this should be considered as a benefit presented by Zr doping. A current compliance of 10-100 μA is used during forming to avoid device shortening and permanent breakdown, so it means that the operation current is limited to these values during forming. The forming process of tantalum oxide bi-layered devices in this kind of structure is normally reported to happen with negative polarity bias over the top electrode. The negative bias attracts positively charged oxygen vacancies from the more conductive

oxygen vacancy reservoir layer (prepared at $pO_2=10^{-3}$ mbar) to the limiting layer prepared at $pO_2=10^{-1}$ mbar and thus immediately promoted the resistance reduction and filament formation (electroforming). Vacancies are also thermally generated by joule heating during electroforming step. In the case of Zr doping devices, some of them already present oxygen vacancy prior to forming at the limiting layer and thus it does not require a severe forming voltage step.

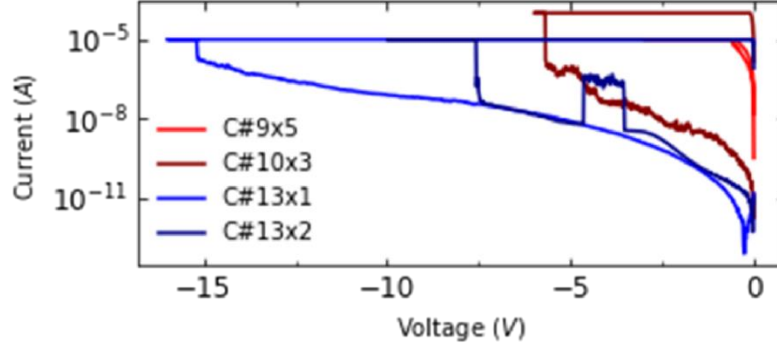


Figure 17: Forming operation for 2 pure tantalum oxide devices (in blue) and 2 Zr doped devices (in red) with 80 μm pad sizes.

According to I-V DC sweep tests, shown in figure 18a, Zr doped tantalum oxide memristors of type Ia (See Table 5) have mean values of $R_{\text{off}}/R_{\text{on}}$ ratio (resistance window) for 10 switching cycles ranging from 7.0 to 13.0 for different devices at the same wafer. Such values are in average higher than the resistance window presented by pure tantalum oxide with structure type Ib that range from 1.3 to 9.5. This can be considered another benefit of Zr doping since high resistance window is an important metric for memristor application as previous discussed.

Voltage operation is another important parameter, high voltage operation leads to increase in energy consumption and circuit requirements. The Zr doped device type Ia is SET (positive cycle) and RESET (negative cycle) with voltage values going from 1.4 to 2.0V, whereas pure tantalum oxide devices structure type Ib are switched with higher voltage values (2.5–3.5V). Thus, for structure type I, Zr doped devices (Ia) presented lower operations voltages compared to pure tantalum oxide devices (Ib).

Regarding resistance operation values (see figure 18), Zr doped devices (Ia) presented a lower resistance value for LRS state compared to pure tantalum oxide devices (Ib), which should be expected once doping increase defect concentration and leakage current. This effect can be considered a drawback since high current operation implies higher energy consumption.

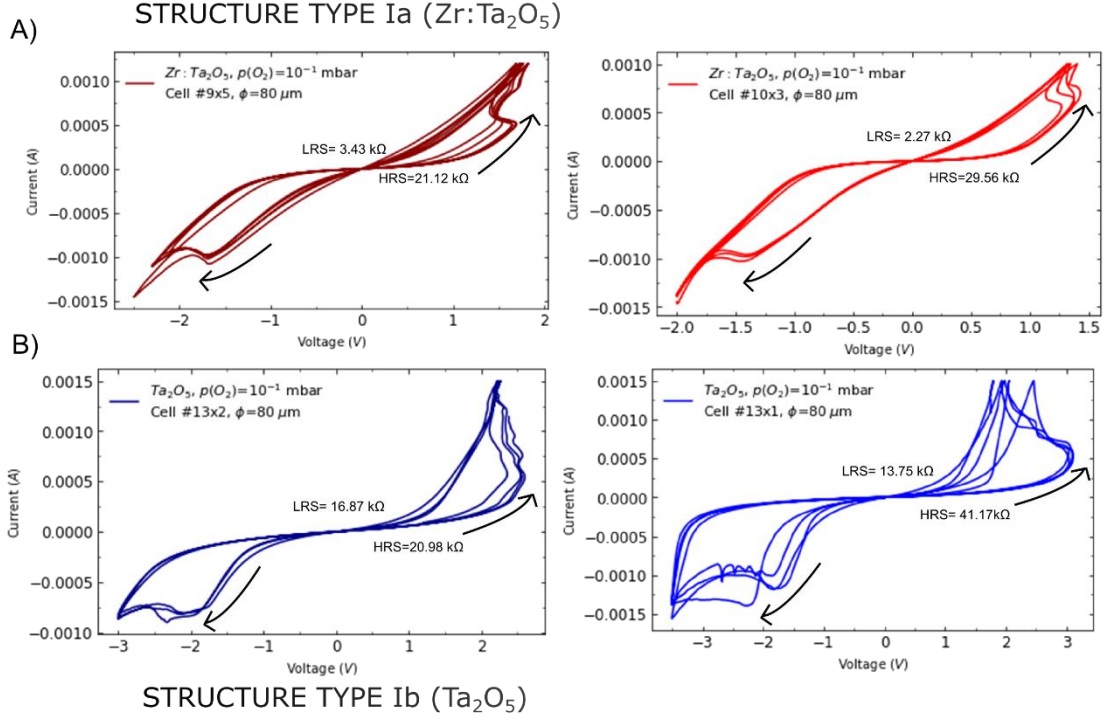


Figure 18: I-V switching cycles of a) different cells (#9x5 and #10x3) at the same wafer of 80 μm pad size Zr doped tantalum oxide device structure type Ia and b) 80 μm pad size, cells #13x2 and #13x1 of pure tantalum oxide-based device structure type Ib.

In summary, regarding switching characteristics, Zr doped devices have generally a lower ON state resistance value compared to pure Ta based devices. Also, a lower switching and forming voltage, and a higher resistance window. Zr doped devices also undergo a more stable and less variable switching with a well-defined hysteresis loop. Cycle to cycle variability analysis in the table 5 showed a lower relative standard error (RSE) of maximum 10% for Zr: Ta₂O₅ devices compared to a maximum RSE value of 20% for non-doped device. As the pure tantalum oxide need a prior forming step in which high voltage is applied in order to start switching, this variability can be ascribed to this random defect formation structure promoted by the high voltage forming step. On the other hand, the lower variability in the resistance values of Zr doped devices may be an evidence of a stable formed filamentary structure probably enhanced by Zr doping interaction with oxygen vacancies [59].

Table 5: Cycle to cycle variability for devices with stack structure type Ia and Ib with 80 μ m pad sizes. See in the table mean resistance values, relative standard error (RSE), resistance window and forming voltage.

	MEAN R. (K Ω)	R. S. E (%)	R_{off}/R_{on}	Forming Voltage (V)
Structure type Ia – 80 μm - Cell#9x5 (Zr:Ta₂O₅) (fig. 19 a)				
ON	3.4	6.9	6.2	-0.5
OFF	21.1	2.7		
Structure type Ia -80μm – Cell#10x3 (Zr:Ta₂O₅) (fig. 19 a)				
ON	2.3	9.9	13.2	-5
OFF	29.6	1.6		
Structure type Ib-80μm – Cell#13x2 (Ta₂O₅) (fig. 19 b)				
ON	16.9	20.1	1.3	-7.5
OFF	21.0	1.4		
Structure type Ib-80μm – Cell#13x1 (Ta₂O₅) (fig. 19 b)				
ON	13.8	14.1	3.0	-15
OFF	41.2	3.1		

5.4.2 Switching characteristics of type II devices

Zr doped devices and pure tantalum oxides prepared at pO_2 of 10^{-2} mbar (oxygen poor atmosphere – type II) have lower forming voltage (maximum V_f of -4V), see fig. 19, compared to films prepared with structure type I showed in the previous section in fig. 17 (V_f of up to -15 V). Some of them are even forming free. It is certainly related to non-stoichiometry and thus to increase of defect content induced by the use of oxygen poor atmosphere during deposition (intrinsic doping) and also to extrinsic doping (Zr). [29], [42], [45]

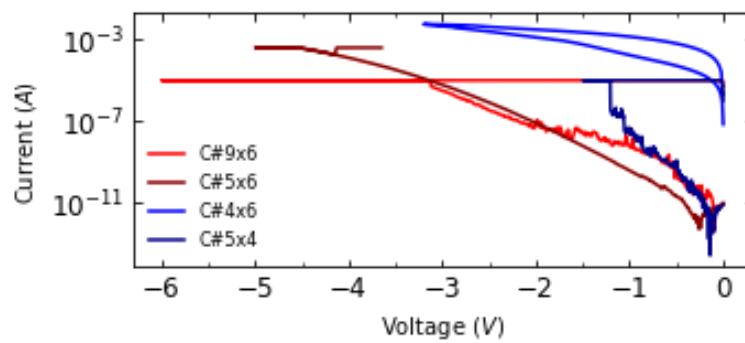


Figure 19: Forming operation for some pure tantalum oxide devices (in blue) and Zr doped devices (in red) with 80 μ m pad sizes.

The current compliance was of 10 and 100 μA adopted to initialize the devices, however as some of them are forming less and start in low resistance state the first operation is of RESET for some devices.

Regarding resistance operation values (LRS and HRS), Zr doped devices (type IIa) have generally a lower LRS value compared to pure Ta based devices (type IIb), as shown in table 6 and in figure 20. For these two devices tested for each structure, Zr doped devices have a LRS ranging from 0.47 k Ω to 2.93 k Ω . On the other hand, pure tantalum oxide devices have LRS going from 2.94 k Ω to 6.11 k Ω . Also, HRS is of maximum 32 and 38 k Ω , respectively (IIa and IIb).

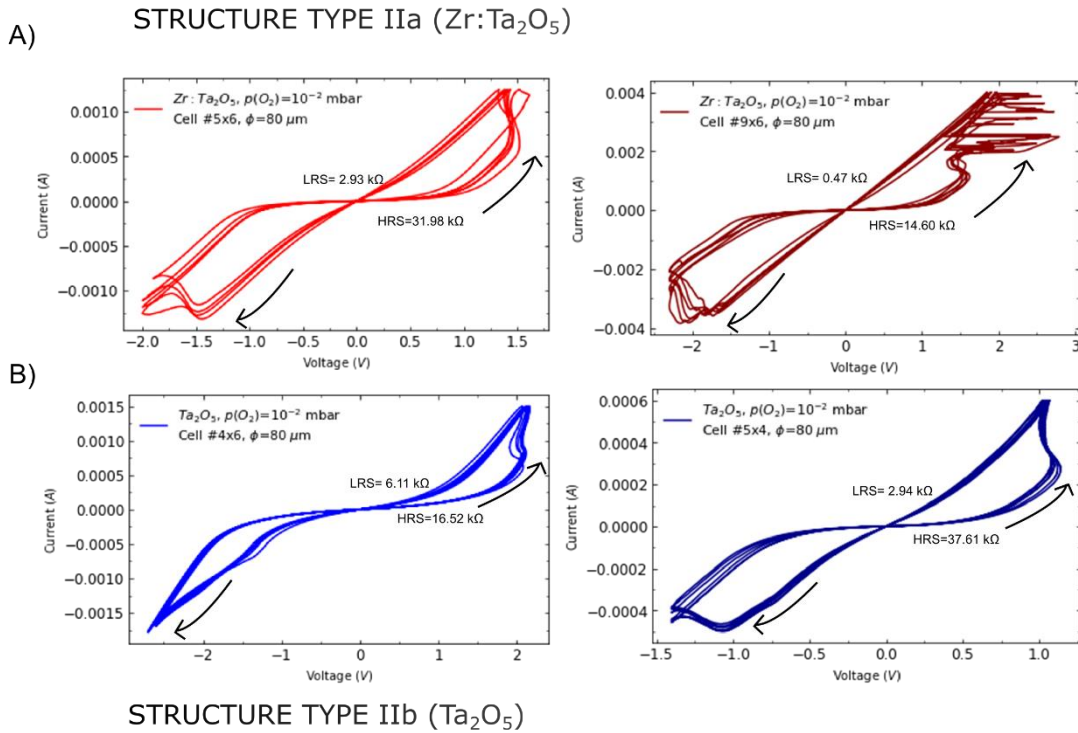


Figure 20: I-V switching cycles of a) 2 different cells (#5x6 and #9x6) of the same die of 80 μm pad size Zr doped tantalum oxide device structure type IIa and b) 80 μm pad size (#4x6 and #5x4) pure tantalum oxide-based device structure type IIb.

It gives to Zr doped devices a higher resistance window of up to 31 compared to maximum 12.8 of pure tantalum oxide see table 6. Cycle to cycle variability of Zr doped devices is a bit higher than the one of pure tantalum oxide devices, but is still reasonable, with a maximum RSE value of 6.2 %.

Regarding scalability, smaller devices of type IIa (Zr doped) with a dog-bone contact structure and active area of $3 \times 3 \mu\text{m}^2$ were tested, as shown in figure 21. To better attest about scalability capability, devices should be produced down to nanometer scale,

however the device active area of the dog-bone structure is many orders of magnitude smaller than the dot pad devices previously analyzed in this work.

Table 6: Cycle to cycle variability for devices with stack structure type IIa and IIb with 80 μ m pad sizes. See in the table mean resistance values, relative standard error (RSE), resistance window and forming voltage.

	MEAN R. (K Ω)	R. S. E (%)	R _{off} /R _{on}	Forming Voltage (V)
Structure type IIa-80μm - Cell#9X6 (Zr:Ta₂O₅) (fig. 19 a)				
ON	0.5	4.5	31.1	-3
OFF	14.6	4.5		
Structure type IIa-80μm – Cell#5X6 (Zr:Ta₂O₅) (fig. 19 a)				
ON	2.9	4.2	10.9	-4
OFF	32.0	6.3		
Structure type IIb-80μm – Cell#4X6 (Ta₂O₅) (fig. 19 b)				
ON	6.1	2.3	2.7	-3
OFF	16.5	0.5		
Structure type IIb-80μm – Cell#5X6 (Ta₂O₅) (fig. 19 b)				
ON	2.94	1.91	12.8	-1.2
OFF	37.61	3.3		

Cross-point devices presented a similar ON resistance state to dot pad devices of 3.6 k Ω but a higher OFF state of 83 K Ω (see figure 21).

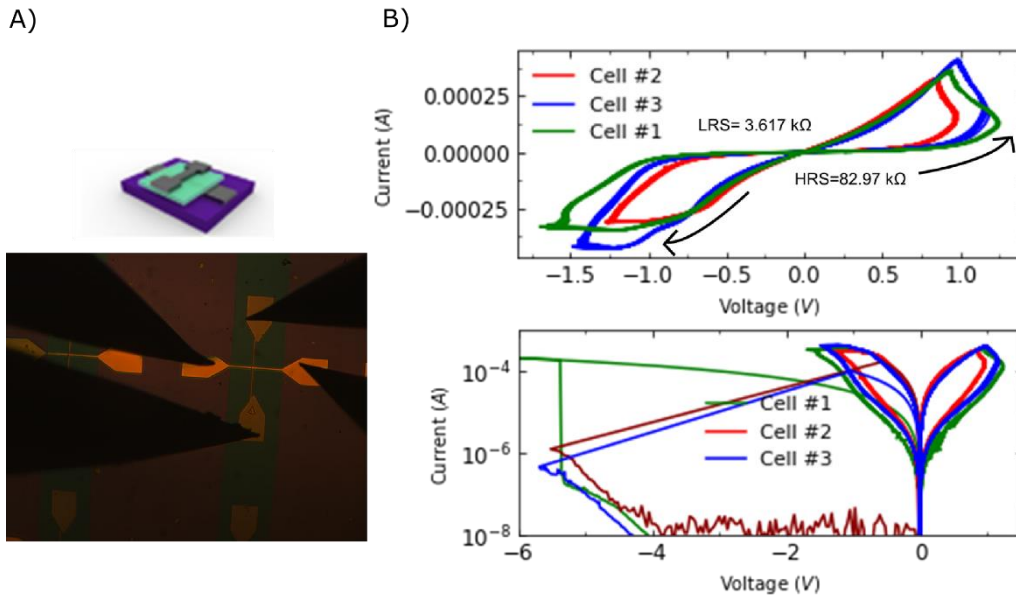


Figure 21: Cross-point type 3 μ m x 3 μ m Zr doped devices (stack structure type IIa) were tested in order to evaluate effect of reduction on device active area. b) It shows a reliable switching behavior, with LRS value of around 3 k Ω and HRS of 83 k Ω .

They have a higher resistance window and present a lower device to device variability, in terms of resistance operation values, since I-V sweep loops of cells #1, #2 and #3 are overlapping each other. They are non-forming free in contrast to some forming less devices with higher pad sizes, but they still have lower forming voltages compared to pure tantalum oxide devices with a much higher active area (pad diameter of 80 μm) and with structure Ib.

The better reliability should indeed be related to the smaller device areas since it suppresses and limits other types of filament configuration or multifilament formation [22]. The higher resistance window may be attributed to heat contribution to RESET operation since smaller pad devices better confine heat and thus contribute to filament dissolution. The heat is more concentrated at the filament in a smaller device. [64], [65]

5.4.3 Electronic transport analysis

As previously discussed on introduction section, electronic transport in tantalum oxide based memristor can be well described by hopping conduction. It's important to emphasize that electronic transport analysis was carried out prior to electroforming process, so these are all pristine devices, in which no conducting filaments were intentionally formed. Current density (J) x Electric field (E) plots of pristine Zr:Ta₂O₅ (Ia) and Ta₂O₅ (Ib) devices along with hopping model adjust are presented in Figure 22. The curves based on the Hopping model (dashed lines) adjust quite well the J-E data of pure and Zr doped tantalum oxide-based devices. According to Ref[37], [38][50] a similar bi-layered tantalum oxide structure is also well described by hopping model. As shown in figure 22, the distance between traps, a , is of 3.5 nm for two pure tantalum oxide-based devices (structure type Ia) with two different pad sizes. It seems reasonable since a similar value of 3.5 nm was also found by Ref. [44][52] for a tantalum oxide film assuming Phonon-assisted trap tunneling (PATT) conduction mechanism. Zr-doped devices with structure type Ib presented a lower distance between traps with values ranging from 1.0 nm to 2.1 nm.

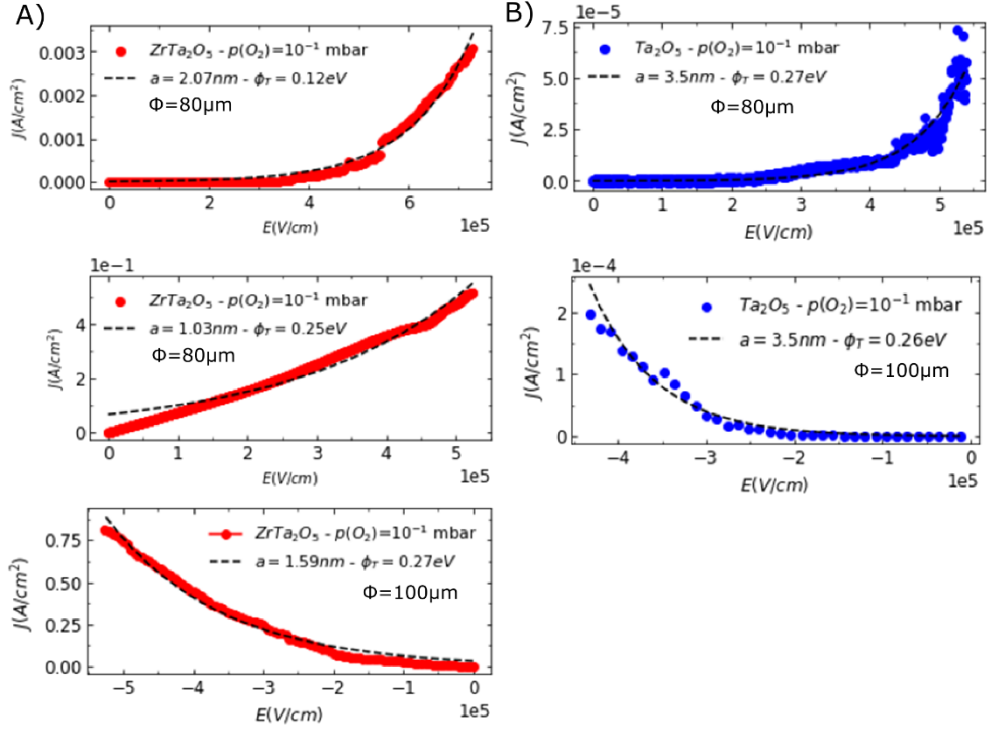


Figure 22: J-E plot of pristine devices along with hopping fit for structure a) Ib and b) Ia with 80 μm and 100 μm pad devices) - a) The devices with pure tantalum oxide films with the limiting layer prepared at 1×10^{-1} mbar (Ib) have a trap distance going of 3.5 nm for the two pad sizes. On the other hand, remarkably b) for the same structure (Ia) and pressure conditions, devices with Zr-doped layers obtained a lower trap distance value of minimum 1.03 nm and maximum 2.07 nm.

This indicates that doping leads to trap formation and thus to a decrease in the distance between traps. Such effect is associate to an increase in leakage current.

In a similar fashion, devices with structure type IIa and IIb, with active layers prepared at lower oxygen partial pressure condition, presented shorter distances between traps of 1.4-1.6 nm for pure tantalum oxide devices and of 0.83-2.0 nm for Zr doped devices, as shown in Figure 23. The decrease in trap distance is related to the increase of the intrinsic defect content, i.e. oxygen vacancies generated by deposition in an oxygen poor atmosphere. Such effect is confirmed by the XPS analysis of the film prepared at low oxygen partial pressure. As Zr doped devices presented an even lower distance between traps it seems reasonable to take into account the defects generated by extrinsic doping (Zr doping). It was evidenced by SE analysis, as in gap-states referred as traps were evidenced in Zr doped films prepared at all oxygen partial pressure conditions.

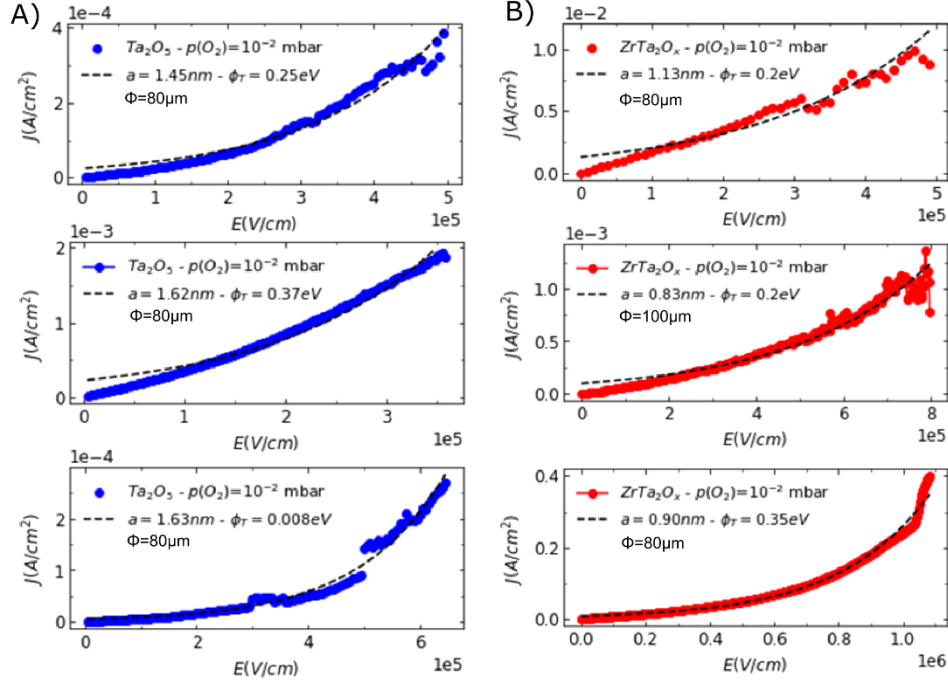


Figure 23: The devices with pure tantalum oxide films with the limiting layer prepared at 2×10^{-2} mbar (IIb) have a trap distance going from 1.45 nm to 1.63 nm. On the other hand, b) for the same structure (IIa) and pressure conditions, devices with Zr-doped layers obtained a lower trap distance value of minimum 0.83 nm.

5.4 Doping effect on vacancy concentration and switching operation parameters

As previously considered by ref. [44][52], the decrease in trap distance, a_{traps} , reflects an increase in defect concentration, N , which is given by:

$$N = a_{traps}^{-1/3}$$

For this work, the defect concentration estimated for devices with switching layers prepared in two different oxygen partial pressure atmosphere, referred as type I ($pO_2 = 10^{-1}$ mbar) and type II ($pO_2 = 10^{-2}$ mbar), accounting for intrinsic doped defects, and finally defects promoted by extrinsic doping (Zr doping), referred as structure Ia and IIa (in red) are shown in Figure 24. The values for the concentration of defects found in the stoichiometric tantalum oxide-based structure (Ia) and non-stoichiometric tantalum oxide device (IIb) are similar to those obtained by Gritensko et al, and Perevalov et al ($1.9 \times 10^{19} \text{ cm}^{-3}$ and $3.0 \times 10^{20} \text{ cm}^{-3}$) by using the Phonon assisted trap tunneling (PATT) model to adjust device IxV curves of devices with non-stoichiometric tantalum oxide active layers [44], [52]. This comparison endorses the methodology adopted in this work. The

concentration values are $2.27 \times 10^{19} \text{ cm}^{-3}$ and $2.73 \times 10^{20} \text{ cm}^{-3}$ for structure type Ib and IIb, respectively. Likewise, Zr doped structures prepared at oxygen poor atmosphere (IIa) and oxygen rich (Ia) atmosphere have a larger defect concentration of $1.33 \times 10^{21} \text{ cm}^{-3}$ and $2.45 \times 10^{20} \text{ cm}^{-3}$.

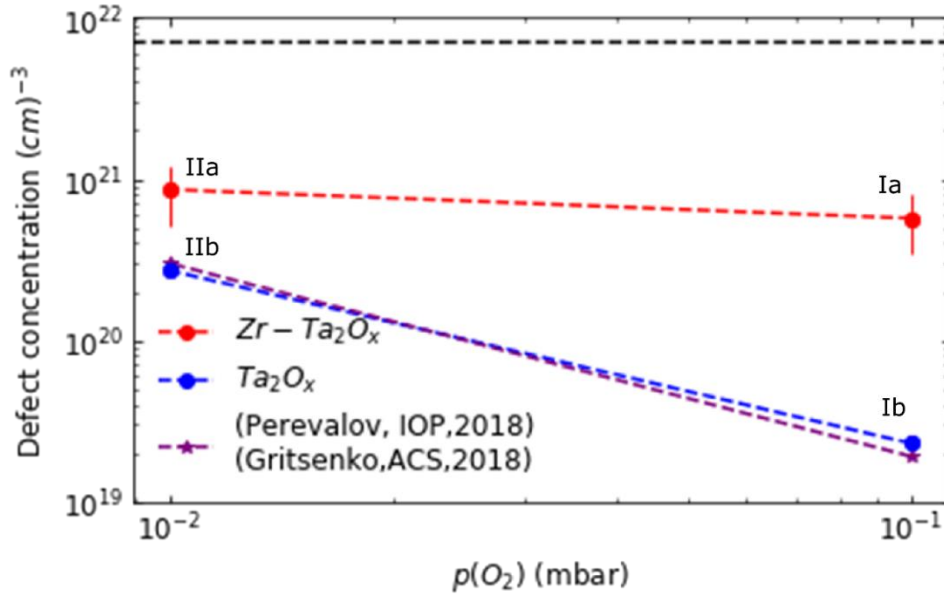


Figure 24: The devices with pure tantalum oxide films have a trap density of $2.27 \times 10^{19} \text{ cm}^{-3}$ (type Ib) and $2.73 \times 10^{20} \text{ cm}^{-3}$ (type IIb). Such variation is associated with the difference in the oxygen stoichiometry and partial reduction of the active layer in both devices that were produced using different oxygen partial pressures. These values are similar to those obtained by Gritsenko et al (in purple) of $1.9 \times 10^{19} \text{ cm}^{-3}$ and $3 \times 10^{20} \text{ cm}^{-3}$ by using the Phonon assisted trap tunneling (PATT) model to adjust device IxV curves [52]. Interestingly, for the devices with Zr-doped layers the obtained trap density values are larger, $2.45 \times 10^{20} \text{ cm}^{-3}$ and $1.33 \times 10^{21} \text{ cm}^{-3}$ for device type Ia and IIa, respectively.

Therefore, it interestingly seems to show that Zr doping can indeed increase defect content (oxygen vacancy content). So, as previously discussed, Zr^{4+} extrinsic doping seems to favor the promotion of oxygen vacancies due to substitution of Ta^{5+} and thus evolution of oxygen to maintain electroneutrality of the system [19], [29], [42], [46]. Same way as using low oxygen partial pressure also promote the formation of sub-stoichiometric oxides which can accommodate oxygen vacancies [10], [45], [48].

It can also relate to change of device behavior: films with defects generated by extrinsic doping (Zr doping – Ia and IIa) and intrinsic doping (IIb) also performed lower forming voltage (see figure 25), compared to the device based on the stoichiometric film structure type Ib. The increase in oxygen vacancy content may result in the increase of current density in pristine devices, and thus contribute to conductive filament formation

and to mitigation of electroforming step [43]. The soft electro-formation process can also contribute to reduction of cycle to cycle and device to device variability (see section 5.1) [45], [56].

Zr doped devices prepared at both oxygen partial pressure conditions presented a higher resistance window compared to pure tantalum oxides (see fig. 26). Zr doped devices have mean resistance window of 23.8 ± 3.6 and 9.6 ± 1.6 for oxygen poor and rich condition, respectively. On the other hand, pure tantalum oxide devices have it going from 7.7 ± 3.6 to 5.7 ± 2.1 , respectively. The increase in the resistance window (ON-OFF ratio) might be associated to the interaction of Zr with oxygen vacancies. As previously attested [11], [59], [66], dopants can interact with oxygen vacancies and can contribute to filament confinement. The dense filament can promote current concentration and local heating which certainly contribute to filament dissolution, gap formation and thus promotion of RESET operation. This unfortunately contribute to increase in conductance state and thus to current operation, which hence might be considered as a drawback effect of doping[46].

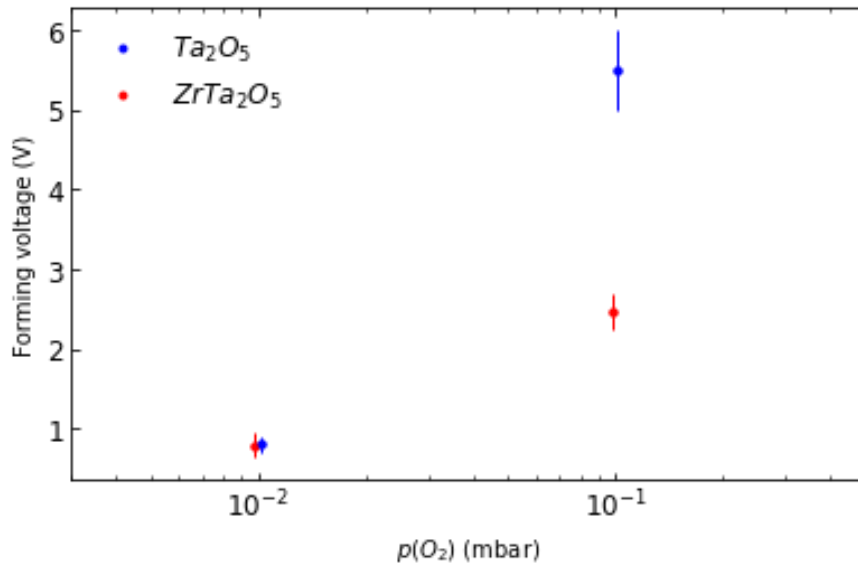


Figure 25: Forming voltage values of extrinsic doped films (Zr doping – Ia and IIa) and intrinsic doped ones (IIa) presented lower forming voltage of $-0.8V \pm 0.16V$, $-1.89V \pm 0.75V$, $-0.803V \pm 0.098V$, respectively, compared to the device based on the stoichiometric film structure type Ib of $-7.475V \pm 1.59V$.

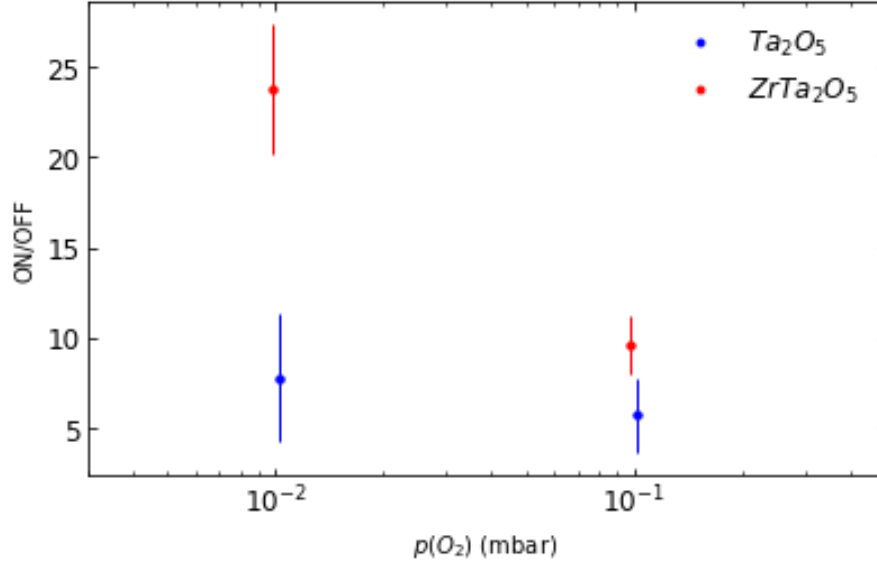


Figure 26: Zr doped devices prepared at both oxygen partial pressure conditions 1×10^{-1} mbar (O_2 rich) and 2×10^{-2} mbar (O_2 poor) presented a higher resistance window of 23.8 ± 3.58 and 9.63 ± 1.61 for oxygen poor and rich condition, compared to pure tantalum oxides structure that have a mean resistance window ranging of 7.74 ± 3.56 and 5.69 ± 2.09 for oxygen poor and rich condition Ta based devices.

5.6 Multi-state analog switching

Synaptic characteristics and weight modulation for neuromorphic computing following well known training protocols as spike timing dependent plasticity are better evaluated in pulses testing routines[34], [67], [68]. DC sweep test is not usually used to evaluate synaptic characteristic, but it instead provides an indication of gradual switching and also can give some hints about operation parameters, etc. Gradual switching is a characteristic required for neuromorphic applications[34], [68]. Gradual analog switching and multistate switching were here observed in pure tantalum oxide and Zr doped tantalum oxide devices, see figure 27. This resistance or weight change in this DC sweep measurements were done by performing a sweep cycle with a voltage stop value below the maximum switching voltage for RESET and SET operations. For these operation conditions, the extrinsic doped device with structure IIb was chosen to evaluate analog gradual switching and multistate switching behavior, see figure 27(a).

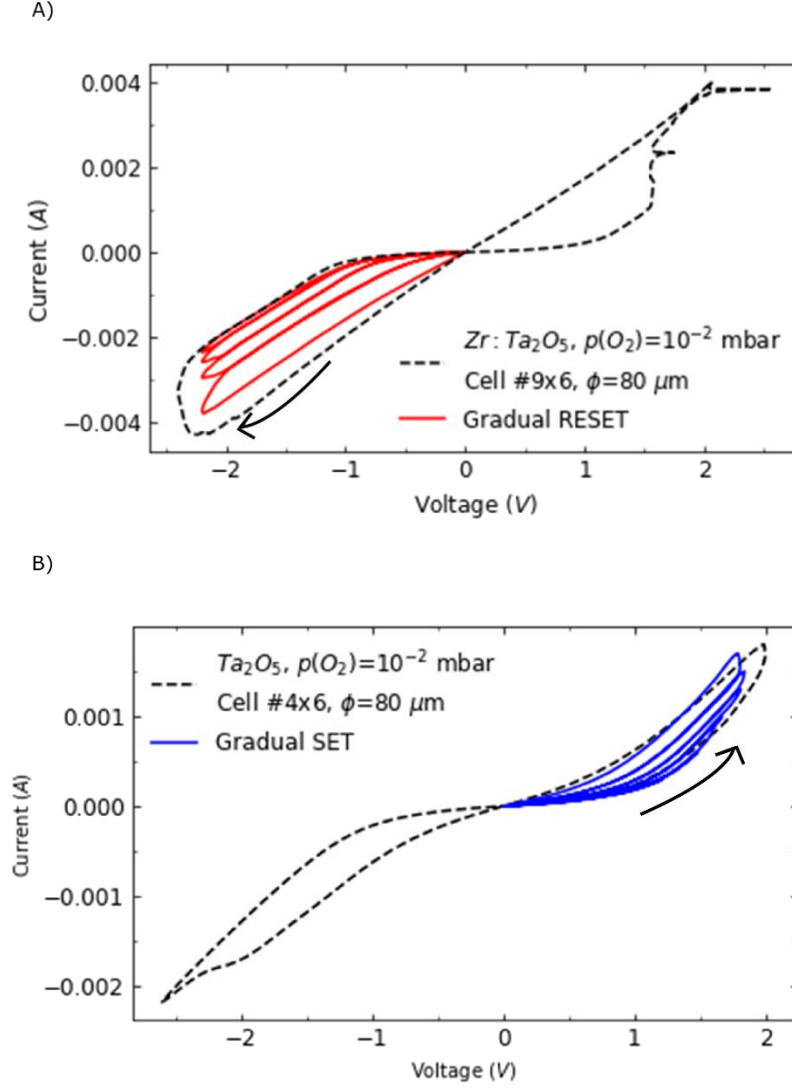


Figure 27: Analog gradual switching operations observed in a) Zr doped devices in negative RESET operations and b) in pure tantalum oxide devices in positive SET operations.

These resistance interstates were accessed by using a lower reset voltage of -2.1 compared to actual RESET voltage of -2.4 V. This procedure was done recursively until complete RESET were done reaching the highest HRS state value for this device of 14.6 k Ω . A total of 5 resistance states were possible to access for this voltage stop of -2.1 V. As shown in figure 27 (a), it goes from 660 Ω (LRS) \rightarrow 3.22 k Ω \rightarrow 8.60 k Ω \rightarrow 12.50 k Ω and finally is completed RESET to 14.60 k Ω (HRS).

Similarly, but now controlling the current compliance, multistate switching was also realized in pure tantalum oxide devices as shown in figure 27 (b). They were accessed by setting different current compliance levels in sequence going from 0.4 mA to 1.5 mA.

condition was attained as a result of a current compliance control of 1.1 mA to 2mA. It was gradually SET and reached the following interstate resistance values 12.95 k Ω (HRS) -> 8.62 k Ω -> 6.77 k Ω -> 4.8 k Ω -> 3.13 k Ω (LRS).

So, it was shown that these proposed tantalum oxide-based device structures follow gradual analog switching with different well resolved multilevel resistance values that can be accessed controlling voltage step or current compliance. Further study with pulsed testing routines should be performed in order to better evaluate synaptic characteristic and also understand doping effect on weight change dynamics.

6. Conclusion

An engineering of defect strategy was proposed to design memristors devices with enhanced performance. the idea is to promote oxygen vacancies by adding zirconium on tantalum oxide and also by controlling the oxygen atmosphere during deposition of the active layer using PLD. By-layered tantalum-oxide-based devices with different combinations of stacks sequences of pure tantalum oxide and Zr doped tantalum oxide were fabricated and tested. Controlling the oxygen partial pressure during growth of the tantalum oxide films and also doping tantalum oxide with zirconia proved to promote oxygen vacancy formation. According to ellipsometry, absorption spectra of pure and Zr doped tantalum oxide film revealed the presence of subgap states which can be attributed to the presence of oxygen vacancies[43], [62]. XPS analysis of pure tantalum oxide film deposited in oxygen poor atmosphere also demonstrate that the oxide is non-stoichiometric and thus oxygen vacancy rich.

It was shown that Zr doping (extrinsic doping) can leads to devices with reduced forming voltage by inducing oxygen vacancy formation by partial substitution of Ta. Similar effect was also obtained by reducing oxygen partial pressure during deposition (intrinsic doping). Vacancies were considered as traps and the distance between them was determined by electronic transport analysis considering hopping conduction. Zr doped devices have indeed a higher oxygen vacancy concentration of up to $1.33 \times 10^{21} \text{ cm}^{-3}$ while pure tantalum oxide reached a maximum oxygen vacancy concentration with intrinsic doping of $2.73 \times 10^{20} \text{ cm}^{-3}$. Zr doped devices also have a higher ON-OFF ratio, up to 28, as compared to pure tantalum oxide devices of maximum 12. They have also lower cycle to cycle variability of up to 10% while-non doped devices have a maximum relative standard error of 20%.

Increase in ON-OFF ratio, reduced forming voltage and increase in reliability are advantageous characteristics promoted by Zr doping of tantalum oxide memristor. The probably explanation to the promotion of oxygen vacancies rely on the substitution of Ta^{5+} by Zr^{4+} which should be accompanied by the evolution of oxygen to keep charge neutrality of the system as previously suggested by ref[19], [42]. Regarding the reduction in variability and increase in resistance window, the reason should be due to Zr interaction with these vacancies, confining the conductive filament and thus restricting the filament

configuration [46], [59]. It was possible to show how defect engineering can be used to tune memristors for different applications and also to suppress application limitations.

These devices undergo analog switching (non-abrupt switching) as well as multistate switching which suggest promising application in neuromorphic computing. Further studies are necessary to attest doping effect on resistance modulation dynamics for neuromorphic computing.

A. Appendices

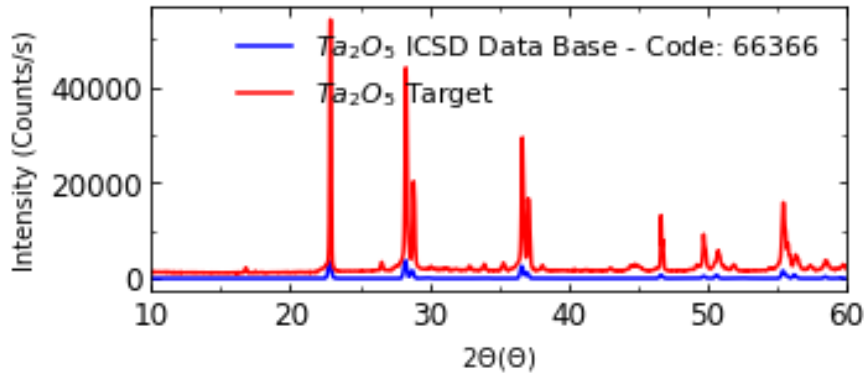
Binding energy constraint used to fit the tantalum oxide thin film XPS data:

Table 7: Tantalum oxide XPS fitting constraints.

Peak	Phase	Binding Energy (eV)	FWHM
Ta4f7 Ta⁽⁰⁾	Ta	21.50 : 21.70	0.5 : 1.0
Ta4f5 Ta⁽⁰⁾	Ta	23.40 : 23.80	1.4 : 2.0
Ta4f7 Ta⁽⁺¹⁾	Ta ₂ O	22.40 : 22.60	1.4 : 1.8
Ta4f5 Ta⁽⁺¹⁾	Ta ₂ O	24.30 : 24.50	1.4 : 1.8
Ta4f7 Ta⁽⁺²⁾	TaO	23.00 : 23.60	1.4 : 1.8
Ta4f5 Ta⁽⁺²⁾	TaO	24.90 : 25.50	1.4 : 1.8
Ta4f7 Ta⁽⁺³⁾	Ta ₂ O ₃	24.10 : 24.50	1.4 : 1.8
Ta4f5 Ta⁽⁺³⁾	Ta ₂ O ₃	26.00 : 26.40	1.4 : 1.8
Ta4f7 Ta⁽⁺⁴⁾	TaO ₂	25.30 : 26.10	1.4 : 1.8
Ta4f5 Ta⁽⁺⁴⁾	TaO ₂	27.10 : 27.90	1.4 : 1.8
Ta4f7 Ta⁽⁺⁵⁾	Ta ₂ O ₅	26.40 : 27.20	1.4 : 1.8
Ta4f5 Ta⁽⁺⁵⁾	Ta ₂ O ₅	28.20 : 30.00	1.4 : 1.8

XRD pattern of the pure and doped tantalum oxide PLD target with β -Ta₂O₅ phase:

A)



B)

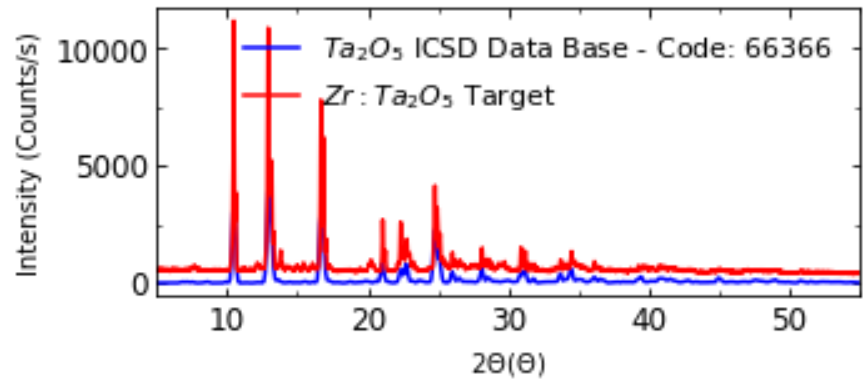


Figure 28: X-ray diffraction pattern of the a) pure tantalum oxide using a copper x-ray target source and b) 20% zirconium oxide and 80% tantalum oxide powder mixture after sintering using molybdenum target source.

Performance results of devices type Ia and Ib with 100 μm pad is presented:

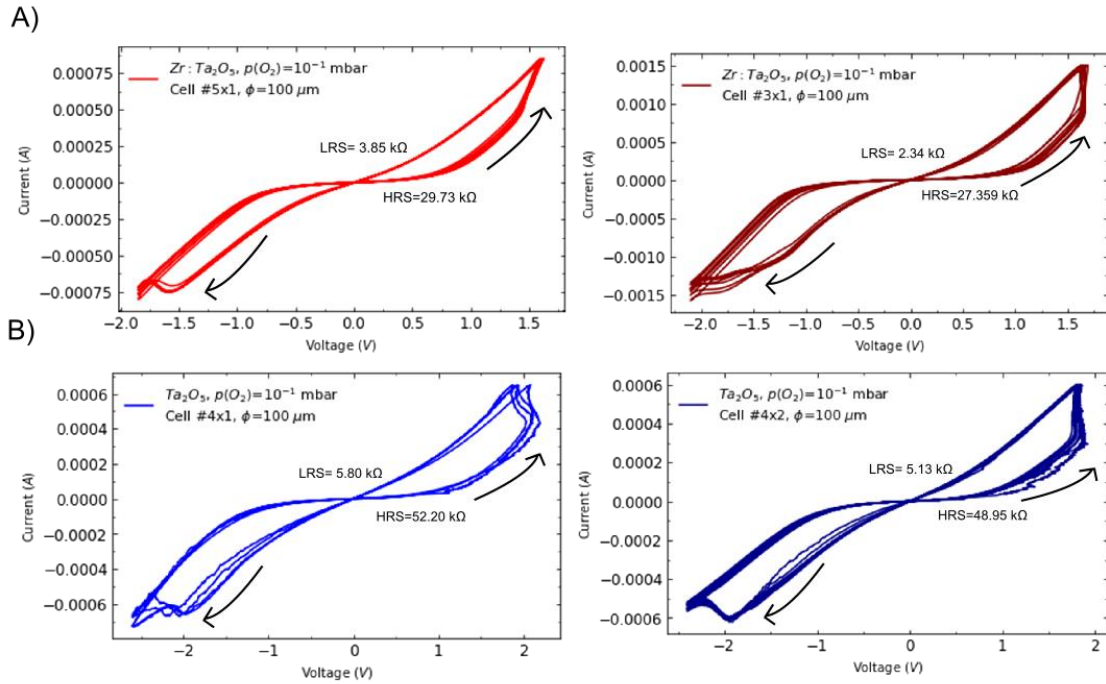


Figure 29:I-V switching cycles of a) 2 different cells (5x1 and 3x1) at the same die of 100 μm pad size Zr doped tantalum oxide device structure type Ia and b) 100 μm (4x1 and 4x2) pure tantalum oxide-based device structure type Ib.

Table 8:Cycle to cycle variability for devices with stack structure type Ia and Ib with 100 μm and 80 μm pad sizes.

Ia-100 μm - Cell#3X1 (Zr doped)				
	MEAN R. (K Ω)	STD ERROR (Ω)	R. STD ERROR (%)	ON-OFF ratio
ON	3.85	44.2	1.90	11.69
OFF	29.74	1239.27	4.53	
Ia-100 μm – Cell#5X1 (Zr doped)				
	MEAN R. (K Ω)	STD ERROR (Ω)	R. STD ERROR (%)	ON-OFF ratio
ON	2.34	50.81	1.32	7.72
OFF	27.36	804.12	2.71	
Ib-100 μm – Cell#4X1 (Pure Ta based)				
	MEAN R. (K Ω)	STD ERROR (Ω)	R. STD ERROR (%)	ON-OFF ratio
ON	5.80	347.05	5.98	9.00
OFF	52.20	2315.85	4.44	
Ib-100 μm – Cell#4X2 (Pure Ta based)				
	MEAN R. (K Ω)	STD ERROR (Ω)	R. STD ERROR (%)	ON-OFF ratio
ON	5.13	203.04	3.96	9.50
OFF	48.95	1267.08	2.59	

Bibliography

- [1] D. S. Jeong, R. Thomas, R. S. Katiyar, J. F. Scott, and H. Kohlstedt, “Emerging memories: resistive switching,” vol. 076502, 2012, doi: 10.1088/0034-4885/75/7/076502.
- [2] Waser R, Aono M. Nanoionics-based resistive switching memories. *Nat Mater.* 2007;6(11):833-840. doi:10.1038/nmat2023
- [3] A. Sawa, “Resistive switching in transition metal oxides,” *Mater. Today*, vol. 11, no. 6, pp. 28–36, 2008, doi: 10.1016/S1369-7021(08)70119-6.
- [4] B. R. Field-, D. Ielmini, S. Member, and A. Resistive, “Modeling the Universal Set / Reset Characteristics of Filament Growth,” vol. 58, no. 12, pp. 4309–4317, 2011.
- [5] W. Kim *et al.*, “Impact of oxygen exchange reaction at the ohmic interface in Ta2O5-based ReRAM devices,” *Nanoscale*, vol. 8, no. 41, pp. 17774–17781, 2016, doi: 10.1039/c6nr03810g.
- [6] C. FERREYRA *et al.*, “Selective activation of memristive interfaces in TaOx-based devices by controlling oxygen vacancies dynamics at the nanoscale,” *Nanotechnology*, 2019.
- [7] K. M. Kim, D. S. Jeong, and C. S. Hwang, “Nanofilamentary resistive switching in binary oxide system; A review on the present status and outlook,” *Nanotechnology*, vol. 22, no. 25, 2011, doi: 10.1088/0957-4484/22/25/254002.
- [8] S. Stathopoulos, A. Khiat, M. Trapatseli, S. Cortese, and A. Serb, “Multibit memory operation of metal-oxide bi-layer memristors,” *Sci. Rep.*, no. November, pp. 1–7, 2017, doi: 10.1038/s41598-017-17785-1.
- [9] H. M. Christen and G. Eres, “Recent advances in pulsed-laser deposition of complex oxides,” *J. Phys. Condens. Matter*, vol. 20, no. 26, 2008, doi: 10.1088/0953-8984/20/26/264005.
- [10] Y. Li *et al.*, “Tuning the stoichiometry and electrical properties of tantalum oxide thin films,” *Appl. Surf. Sci.*, vol. 470, no. June 2018, pp. 1071–1074, 2019, doi: 10.1016/j.apsusc.2018.11.153.
- [11] S. Kim, S. Choi, J. Lee, W. D. Lu, and K. I. M. E. T. Al, “Tuning Resistive Switching Characteristics of Tantalum Oxide Memristors through Si Doping,” , *ACS nano*, 2014.
- [12] K. Kukli *et al.*, “Atomic layer deposition and properties of mixed Ta2O5 and ZrO2

- films,” *AIP Adv.*, vol. 7, no. 2, 2017, doi: 10.1063/1.4975928.
- [13] D. B. Strukov, G. S. Snider, D. R. Stewart, and R. S. Williams, “The missing memristor found,” vol. 453, no. May, pp. 80–84, 2008, doi: 10.1038/nature06932.
 - [14] L. Chua, “Memristor-The missing circuit element,” in *IEEE Transactions on Circuit Theory*, vol. 18, no. 5, pp. 507–519, September 1971, doi: 10.1109/TCT.1971.1083337.
 - [15] L. Chua, “Everything You Wish to Know About Memristors But Are Afraid to Ask,” vol. 24, no. 2, pp. 319–368, 2015, doi: 10.13164/re.2015.0319.
 - [16] S. H. Jo, T. Chang, I. Ebong, B. B. Bhadviya, P. Mazumder, and W. Lu, “Nanoscale memristor device as synapse in neuromorphic systems,” *Nano Lett.*, vol. 10, no. 4, pp. 1297–1301, 2010, doi: 10.1021/nl904092h.
 - [17] S. Menzel, U. Böttger, M. Wimmer, and M. Salinga, “Physics of the Switching Kinetics in Resistive Memories,” pp. 6306–6325, 2015, doi: 10.1002/adfm.201500825.
 - [18] J. S. Lee, S. Lee, T. W. Noh, J. S. Lee, S. Lee, and T. W. Noh, “Resistive switching phenomena : A review of statistical physics approaches Resistive switching” vol. 031303, 2015, doi: 10.1063/1.4929512.
 - [19] R. Schmitt, J. Spring, R. Korobko, and J. L. M. Rupp, “Design of Oxygen Vacancy Configuration for Memristive Systems,” *ACS Nano*, vol. 11, no. 9, pp. 8881–8891, 2017, doi: 10.1021/acsnano.7b03116.
 - [20] X. L. Jiang *et al.*, “Characteristics of different types of filaments in resistive switching memories investigated by complex impedance spectroscopy,” *Appl. Phys. Lett.*, vol. 102, no. 25, pp. 1–6, 2013, doi: 10.1063/1.4812811.
 - [21] J. E. Stevens, A. J. Lohn, S. A. Decker, B. L. Doyle, P. R. Mickel, and M. J. Marinella, “ Reactive sputtering of substoichiometric Ta₂O_x for resistive memory applications ,” *J. Vac. Sci. Technol. A Vacuum, Surfaces, Film.*, vol. 32, no. 2, p. 021501, 2014, doi: 10.1116/1.4828701.
 - [22] M. Lanza *et al.*, “Recommended Methods to Study Resistive Switching Devices,” *Adv. Electron. Mater.*, vol. 5, no. 1, pp. 1–28, 2019, doi: 10.1002/aelm.201800143.
 - [23] J. J. Yang *et al.*, “High switching endurance in TaOx memristive devices,” vol. 232102, no. 2010, pp. 12–15, 2013, doi: 10.1063/1.3524521.
 - [24] A. C. Torrezan, J. P. Strachan, G. Medeiros-ribeiro, and R. S. Williams, “Sub-nanosecond switching of a tantalum oxide memristor,” vol. 485203, doi: 10.1088/0957-4484/22/48/485203.

- [25] E. Diagram and M. Phases, “The O-Ta (Oxygen-Tantalum) System,” vol. 17, no. 1, pp. 63–77, 1996.
- [26] A. J. Lohn, J. E. Stevens, P. R. Mickel, and M. J. Marinella, “Optimizing TaOx memristor performance and consistency within the reactive sputtering ‘forbidden region,’” *Appl. Phys. Lett.*, vol. 103, no. 6, 2013, doi: 10.1063/1.4817927.
- [27] G. S. Park *et al.*, “In situ observation of filamentary conducting channels in an asymmetric Ta₂O_{5-x}/TaO_{2-x} bilayer structure,” *Nat. Commun.*, vol. 4, pp. 1–9, 2013, doi: 10.1038/ncomms3382.
- [28] H. Jiang and D. A. Stewart, “Using Dopants to Tune Oxygen Vacancy Formation in Transition Metal Oxide Resistive Memory,” 2017, doi: 10.1021/acsami.7b00139.
- [29] H. Yildirim and R. Pachter, “ Extrinsic Dopant Effects on Oxygen Vacancy Formation Energies in ZrO₂ with Implication for Memristive Device Performance ,” *ACS Appl. Electron. Mater.*, vol. 1, no. 4, pp. 467–477, 2019, doi: 10.1021/acsaelm.8b00090.
- [30] S. A. Lee *et al.*, “Phase transitions via selective elemental vacancy engineering in complex oxide thin films,” *Nat. Publ. Gr.*, no. January, pp. 1–10, 2016, doi: 10.1038/srep23649.
- [31] Y. Abbas, A. S. Sokolov, Y. R. Jeon, S. Kim, B. Ku, and C. Choi, “Structural engineering of tantalum oxide based memristor and its electrical switching responses using rapid thermal annealing,” *J. Alloys Compd.*, vol. 759, pp. 44–51, 2018, doi: 10.1016/j.jallcom.2018.05.106.
- [32] Y. Sun *et al.*, “A Ti / AlO_x / TaO_x / Pt Analogue Synapse for Memristive Neural Network,” vol. 3106, no. c, pp. 1–4, 2018, doi: 10.1109/LED.2018.2860053.
- [33] “Xiao-2019-Resistive Random Access Memory Cells with a Bilayer.pdf.” .
- [34] S. Kim, Y. Abbas, Y. R. Jeon, A. S. Sokolov, B. Ku, and C. Choi, “Engineering synaptic characteristics of TaO_x/HfO₂ bi-layered resistive switching device,” *Nanotechnology*, vol. 29, no. 41, 2018, doi: 10.1088/1361-6528/aad64c.
- [35] M. Lee *et al.*, “A fast, high-endurance and scalable non-volatile memory device made from asymmetric Ta₂O_{5-x}/TaO_{2-x} bilayer structures,” *Nat. Mater.*, vol. 10, no. 8, pp. 625–630, 2011, doi: 10.1038/nmat3070.
- [36] F. C. Chiu, “A review on conduction mechanisms in dielectric films,” *Adv. Mater. Sci. Eng.*, vol. 2014, 2014, doi: 10.1155/2014/578168.
- [37] Y. Zhang, N. Deng, H. Wu, Z. Yu, J. Zhang, and H. Qian, “Metallic to hopping

- conduction transition in Ta₂O_{5-x}/TaO_y resistive switching device,” *Appl. Phys. Lett.*, vol. 105, no. 6, pp. 1–5, 2014, doi: 10.1063/1.4893325.
- [38] C. E. Graves, N. Dávila, E. J. Merced-Grafals, S. T. Lam, J. P. Strachan, and R. S. Williams, “Temperature and field-dependent transport measurements in continuously tunable tantalum oxide memristors expose the dominant state variable,” *Appl. Phys. Lett.*, vol. 110, no. 12, 2017, doi: 10.1063/1.4978757.
- [39] A. A. Sharma, M. Noman, M. Abdelmoula, M. Skowronski, and J. A. Bain, “Electronic instabilities leading to electroformation of binary metal oxide-based resistive switches,” *Adv. Funct. Mater.*, vol. 24, no. 35, pp. 5522–5529, 2014, doi: 10.1002/adfm.201400461.
- [40] B. Xiao and S. Watanabe, “Oxygen vacancy effects on an amorphous-TaO_x-based resistance switch: A first principles study,” *Nanoscale*, vol. 6, no. 17, pp. 10169–10178, 2014, doi: 10.1039/c4nr02173h.
- [41] S. Zaima, “Conduction Mechanism of Leakage Current in Ta₂O₅ Films on Si Prepared by LPCVD,” *J. Electrochem. Soc.*, vol. 137, no. 9, p. 2876, 1990, doi: 10.1149/1.2087091.
- [42] H. Jiang and D. A. Stewart, “Using Dopants to Tune Oxygen Vacancy Formation in Transition Metal Oxide Resistive Memory,” *ACS Appl. Mater. Interfaces*, vol. 9, no. 19, pp. 16296–16304, 2017, doi: 10.1021/acsami.7b00139.
- [43] V. A. Gritsenko *et al.*, “Nanoscale potential fluctuations in nonstoichiometric tantalum oxide,” *Nanotechnology*, vol. 29, no. 42, 2018, doi: 10.1088/1361-6528/aad430.
- [44] V. A. Gritsenko *et al.*, “Charge Transport and the Nature of Traps in Oxygen Deficient Tantalum Oxide,” *ACS Appl. Mater. Interfaces*, vol. 10, no. 4, pp. 3769–3775, 2018, doi: 10.1021/acsami.7b16753.
- [45] K. Skaja, M. Andrä, V. Rana, R. Waser, R. Dittmann, and C. Baeumer, “Reduction of the forming voltage through tailored oxygen non-stoichiometry in tantalum oxide ReRAM devices,” *Sci. Rep.*, vol. 8, no. 1, pp. 1–7, 2018, doi: 10.1038/s41598-018-28992-9.
- [46] S. M. Park, H. G. Hwang, J. U. Woo, W. H. Lee, S. J. Chae, and S. Nahm, “Improvement of Conductance Modulation Linearity in a Cu²⁺-Doped KNbO₃ Memristor through the Increase of the Number of Oxygen Vacancies,” *ACS Appl. Mater. Interfaces*, vol. 12, no. 1, pp. 1069–1077, 2020, doi: 10.1021/acsami.9b18794.

-
- [47] J. J. Ke *et al.*, “Surface-Controlled Metal Oxide Resistive Memory,” *IEEE Electron Device Lett.*, vol. 36, no. 12, pp. 1307–1309, 2015, doi: 10.1109/LED.2015.2493343.
- [48] M. T. Brumbach *et al.*, “Evaluating tantalum oxide stoichiometry and oxidation states for optimal memristor performance,” *J. Vac. Sci. Technol. A Vacuum, Surfaces, Film.*, vol. 32, no. 5, p. 051403, 2014, doi: 10.1116/1.4893929.
- [49] R. Schmitt, J. Spring, R. Korobko, and J. L. M. Rupp, “Design of Oxygen Vacancy Configuration for Memristive Systems,” 2017, doi: 10.1021/acsnano.7b03116.
- [50] I. Goldfarb and R. S. Williams, “Conduction centers in a Ta₂O₅- δ Fermi glass,” *Appl. Phys. A Mater. Sci. Process.*, vol. 114, no. 2, pp. 287–289, 2014, doi: 10.1007/s00339-013-8162-9.
- [51] J. Lee, W. Schell, X. Zhu, E. Kioupakis, and W. D. Lu, “Charge Transition of Oxygen Vacancies during Resistive Switching in Oxide-Based RRAM,” *ACS Appl. Mater. Interfaces*, vol. 11, no. 12, pp. 11579–11586, 2019, doi: 10.1021/acsaami.8b18386.
- [52] T. V. Perevalov *et al.*, “Electronic structure and charge transport in nonstoichiometric tantalum oxide,” *Nanotechnology*, vol. 29, no. 26, pp. 2–11, 2018, doi: 10.1088/1361-6528/aaba4c.
- [53] I. Goldfarb *et al.*, “Electronic structure and transport measurements of amorphous transition-metal oxides: Observation of Fermi glass behavior,” *Appl. Phys. A Mater. Sci. Process.*, vol. 107, no. 1, pp. 1–11, 2012, doi: 10.1007/s00339-012-6856-z.
- [54] S. Kumar *et al.*, “Conduction Channel Formation and Dissolution Due to Oxygen Thermophoresis/ Diffusion in Hafnium Oxide Memristors,” 2016, doi: 10.1021/acsnano.6b06275.
- [55] W. Kim, S. Il Park, Z. Zhang, and S. Wong, “Current conduction mechanism of nitrogen-doped AlO_x RRAM,” *IEEE Trans. Electron Devices*, vol. 61, no. 6, pp. 2158–2163, 2014, doi: 10.1109/TED.2014.2319074.
- [56] N. Sedghi *et al.*, “Enhanced switching stability in Ta₂O₅ resistive RAM by fluorine doping,” *Appl. Phys. Lett.*, vol. 111, no. 9, 2017, doi: 10.1063/1.4991879.
- [57] N. Xiao *et al.*, “Resistive Random Access Memory Cells with a Bilayer TiO₂/SiO₂ Insulating Stack for Simultaneous Filamentary and Distributed Resistive Switching,” *Adv. Funct. Mater.*, vol. 27, no. 33, pp. 1–13, 2017, doi: 10.1002/adfm.201700384.

- [58] M. Lübben *et al.*, “Design of defect-chemical properties and device performance in memristive systems,” *Sci. Adv.*, vol. 6, no. 19, 2020, doi: 10.1126/sciadv.aaz9079.
- [59] S. H. Misha *et al.*, “Effect of nitrogen doping on variability of TaOx-RRAM for low-power 3-bit MLC applications,” *ECS Solid State Lett.*, vol. 4, no. 3, pp. P25–P28, 2015, doi: 10.1149/2.0011504ssl.
- [60] H. Fujiwara, *Spectroscopic Ellipsometry Principles and Applications*. .
- [61] R. Grigorovici and A. Vancu, “Optical Properties and Electronic Structure of Amorphous Germanium,” vol. 627, pp. 627–637, 1966.
- [62] T. V. Perevalov, D. R. Islamov, and I. G. Chernykh, “Atomic and Electronic Structures of Intrinsic Defects in Ta2O5: Ab Initio Simulation,” *JETP Lett.*, vol. 107, no. 12, pp. 761–765, 2018, doi: 10.1134/S0021364018120111.
- [63] Y. Guo and J. Robertson, “Comparison of oxygen vacancy defects in crystalline and amorphous Ta2O5,” *Microelectron. Eng.*, vol. 147, pp. 254–259, 2015, doi: 10.1016/j.mee.2015.04.065.
- [64] X. Sheng *et al.*, “Low-Conductance and Multilevel CMOS-Integrated Nanoscale Oxide Memristors,” vol. 1800876, pp. 1–8, 2019, doi: 10.1002/aelm.201800876.
- [65] S. Kumar and R. S. Williams, “domains caused by nonlinear electronic instabilities,” no. 2018, pp. 1–9, 1963, doi: 10.1038/s41467-018-04452-w.
- [66] W. Banerjee, Q. Liu, and H. Hwang, “Engineering of defects in resistive random access memory devices,” *J. Appl. Phys.*, vol. 127, no. 5, 2020, doi: 10.1063/1.5136264.
- [67] W. Wu *et al.*, “Suppress variations of analog resistive memory for neuromorphic computing by localizing Vo formation Suppress variations of analog resistive memory for neuromorphic computing by localizing V o formation,” vol. 152108, 2018, doi: 10.1063/1.5037896.
- [68] Y. Abbas, Y. R. Jeon, A. S. Sokolov, S. Kim, B. Ku, and C. Choi, “Compliance-Free, Digital SET and Analog RESET Synaptic Characteristics of Sub-Tantalum Oxide Based Neuromorphic Device,” *Sci. Rep.*, vol. 8, no. 1, pp. 18–21, 2018, doi: 10.1038/s41598-018-19575-9.